

4. Profiling simple obstacles with the Can-Can

In this paragraph, obstacles with known dimensions and shapes will be profiled with the Can-Can Machine. These obstacles will be profiled to determine the level of accuracy obtainable with the use of the Can-Can Machine. The accuracy of the Can-Can was determined by comparing the Can-Can profile of an obstacle with the actual profile.

4.1. Discrete bumps

Discrete bumps and holes were profiled with the Can-Can Machine at the Gerotek test facilities. These obstacles are permanent and offer repeatability.

4.1.1. 100 mm semi-circular bump

The 100 mm semi-circle bump is a bump constructed out of steel and is used in the testing of suspensions on military vehicles or any all-terrain vehicle. The semi-circle bump is mounted on a 12 mm base plate so that it may be bolted to the ground. The base plate also strengthens the semi-circle. Handles were placed on the side of the bump for easy movement. Figure 56 shows the 100 mm bump.



Figure 56: 100 mm semi-circular bump.

Figure 57 shows the difference between the profiled bump and the actual bump. The profiled bump shows a small distortion in the profile. The distortion was caused due to part of the arm coming into contact with the bump and moving over the bump. Due to the contact between the arm and the bump the arm was raised instead of the arm being elevated by the wheel as the wheel travelled over the bump.

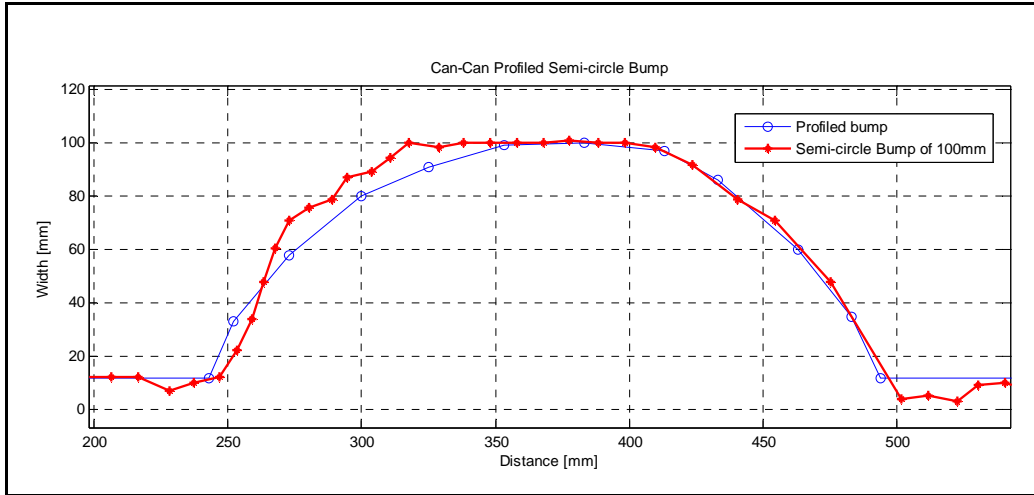


Figure 57: Profiled and actual 100 mm bump.

Although measurements are taken at constant horizontal intervals of 10.18 mm, the horizontal (X) data points are not equally spaced due to the effect of the arm's angle described in Figure 27. The horizontal distance between data points are therefore compressed as the arm rotates upward and again expands as the arm moves down after the crown of the obstacle.

The calculated RMS value of the vertical height of the bump was 55.42 mm and the RMS value of the profile was equal to 52.48 mm. The RMSE between the actual profile and the Can-Can profile was calculated to be 8.96 mm. The RMSE was higher than expected due to the contact between the middle of the arm and the obstacle as previously described. The RMSE and overall correlation obtained between the profiled bump and the actual bump was satisfactory. The error between the profiled bump and the actual bump in Figure 57 is exaggerated due to the difference in the x and y axis scaling.

4.1.2. Parallel and angled corrugations

The parallel and angled corrugations are used in simulating a corrugated gravel road with 25 mm bumps. The corrugation tracks are set in concrete to provide repeatability in any weather without the surface changing or deteriorating. The corrugation tracks are 4 m wide and 100 m in length. The Can-Can Machine profiled the terrain without any of its wheels on the profiled terrain. This increased the accuracy of the profile due to the fact that there was no vertical movement of the profilometer. The profiles of the corrugations were very representative of the actual bump and a profile of a single corrugation bump is shown in Figure 58.

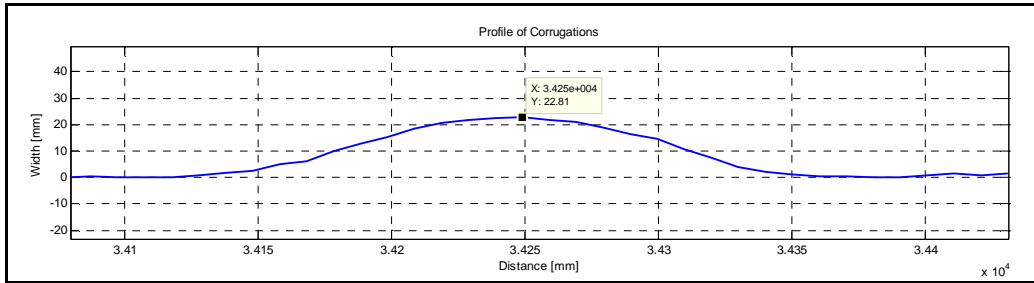


Figure 58: Profile of a corrugation bump.

The vertical RMS values of the actual bump and the profiled bumps could not be compared as the actual dimensions of each bump varied to some extent and were not constant. The profiled height of the corrugations were profiled at 20-26 mm where as the actual corrugations were alleged to be 25 mm.

The actual parallel and angled corrugations are shown in Figure 59 and Figure 61 respectively. Sections of the full profiles of the parallel and angled corrugations are shown in Figure 60 and Figure 62 respectively. The corrugation tracks were built at a slight sideways slant to facilitate water drainage as seen in the profiles.

The profiles of the corrugations were satisfactory as they were visually very representative of the actual tracks and the profiled bumps were within a tolerance of 5 mm of the alleged 25 mm. The deviations in the height of the bumps were as a result of years of testing large military vehicles on the track.

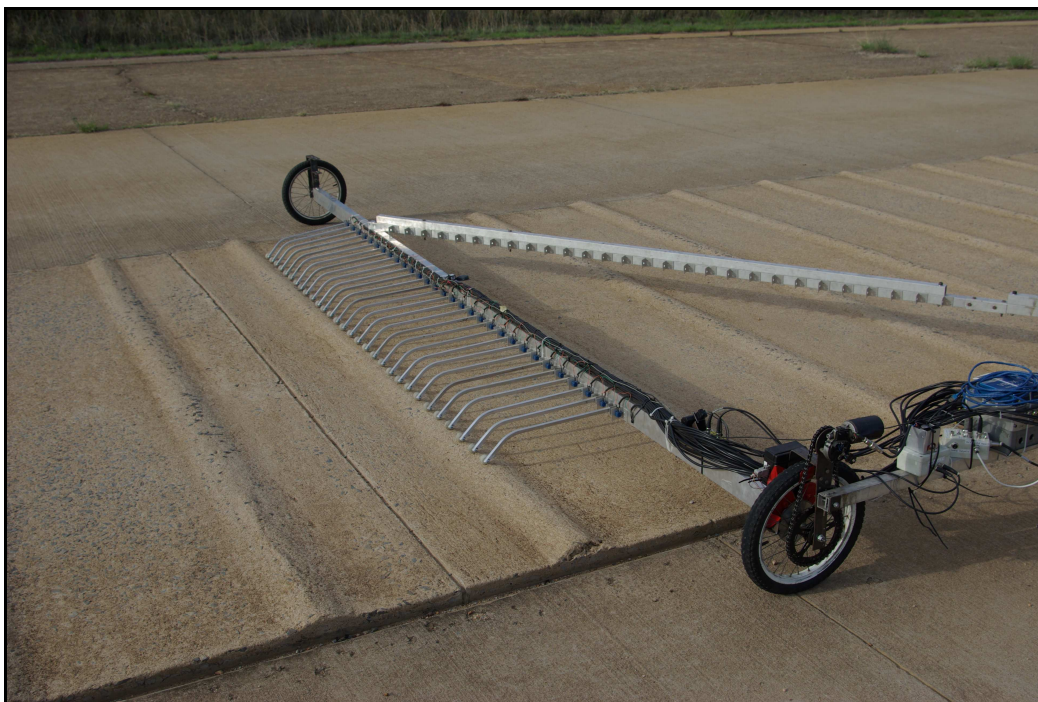


Figure 59: Parallel corrugations at Gerotek.

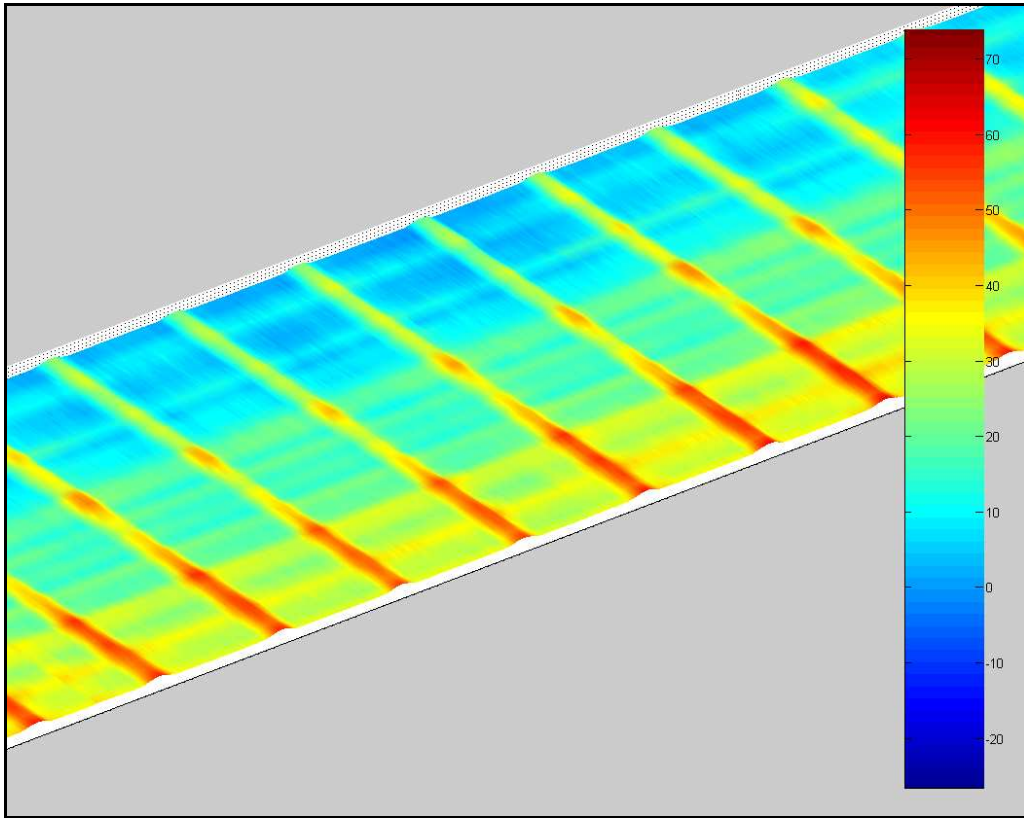


Figure 60: Profiled parallel corrugations.



Figure 61: Angled corrugations at Gerotek.

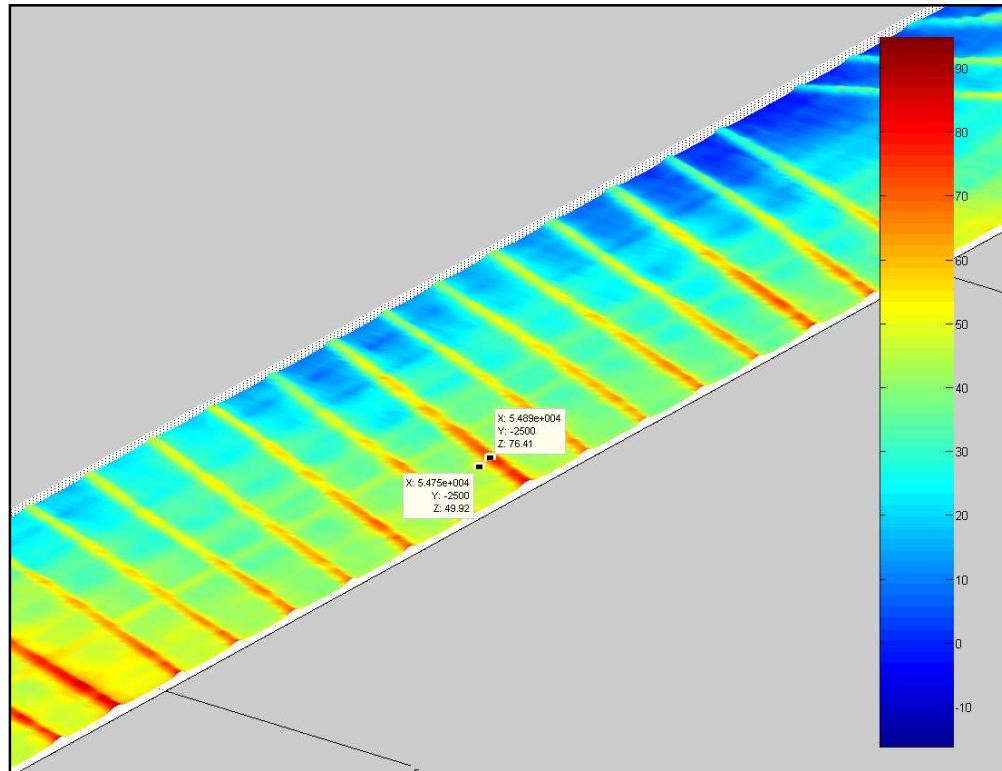


Figure 62: Profiled angled corrugations.

4.1.3. Pot-Holes

The pothole track at the Gerotek test facilities is used for testing the capability of a military vehicle's suspension and steering links in withstanding the input forces into the suspension by driving through 80 mm deep potholes in the road. The profile's accuracy was confirmed in Figure 63, where the actual profile was evaluated and compared with the profiled pothole.

The profile appears rough due to the scale of the graph. The rounded edge in the Can-Can profile is caused by the motion of the small wheels at the end of the arms, which provide a smoother transition over the edge.

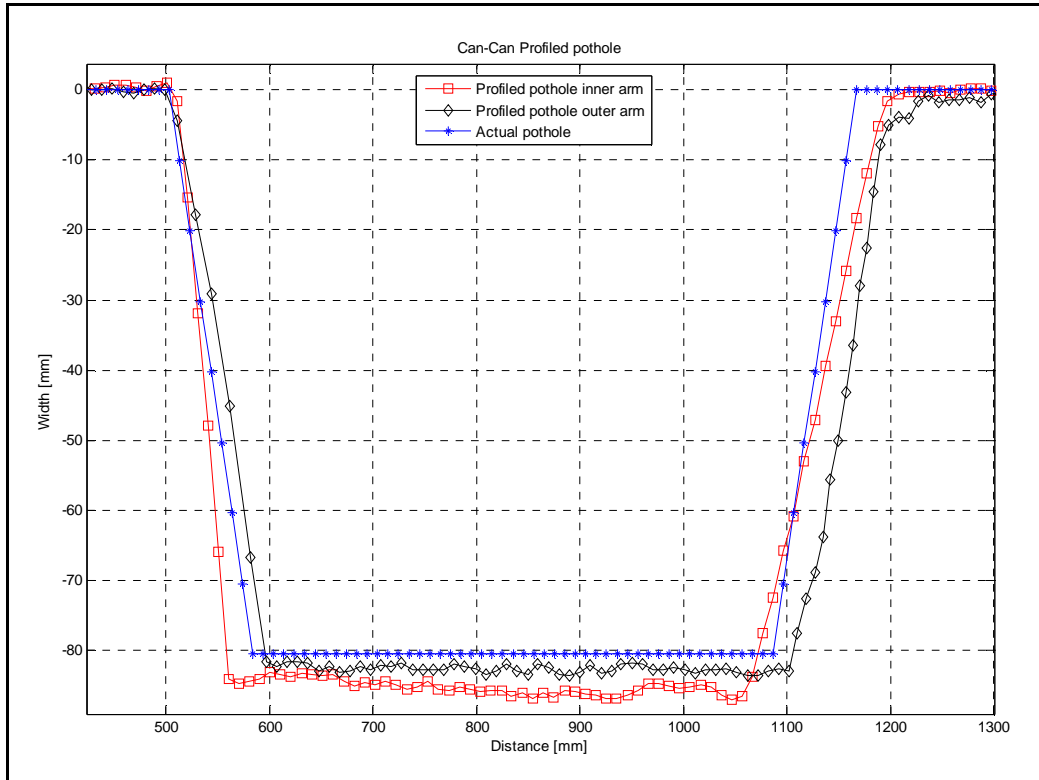


Figure 63: The actual profile and the Can-Can profile of the pothole.

The rounded top edge on the profile of the pothole is also due to wear on the actual pothole. The RMS value of the actual pothole is 46.344 mm and the RMS value of the inner and outer arms is 41.291 mm and 39.497 mm respectively. The RMSE of the profiles is 7.43 mm for the inner arm and 4.28 mm for the outer arm. The profile from the inner arm is deeper as each pothole is sloped towards the inside of the track to assist water drainage. This slope caused the higher RMSE calculated for the inner pothole profile. The difference in the slope of the walls of the inner and outer pothole profiles were due to the construction of the pothole. The profiles of the base of the pothole are rough due to sand and small stones in the actual pothole during profiling. Figure 64 and Figure 65 shows the actual pothole and the profiled pothole tracks respectively. The profile obtained from the Can-Can Machine is accurate and is a good representation of the pothole track. The 35X35 mm mesh grid covering the drain in the pothole is visible in Figure 65.



Figure 64: Pothole track at Gerotek.

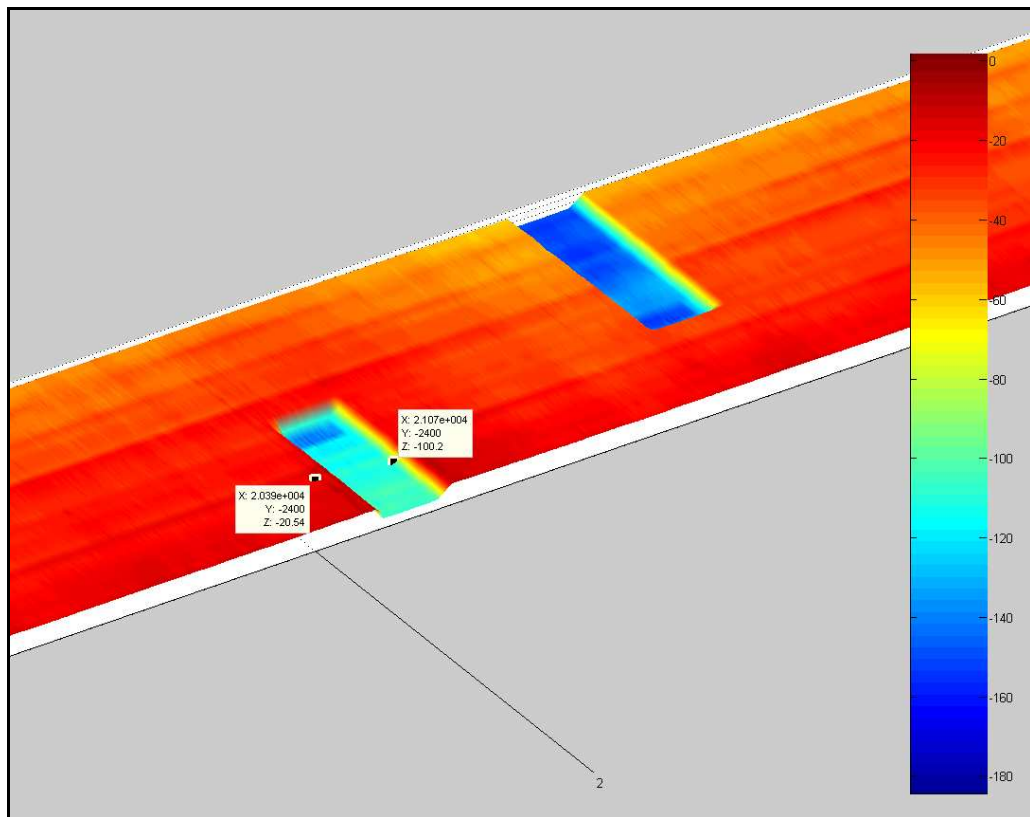


Figure 65: Profiled pothole track.

4.2. Summary on discrete bumps

The discrete bumps were profiled in an attempt to validate the accuracy of the Can-Can Machine. The so called actual bumps used in the graphs were theoretically representative of the bumps used during the tests. The theoretical bumps were generated with the information supplied by the test facility. Due to years of constant testing of large military vehicles at the test facilities deviations between the actual and theoretical bumps were expected.

Deviations in the profile of the 100 mm semi-circle bump were due to the arms making contact with the obstacle. This may be avoided with the adjustment of the curve and angle of the arms. Deviations in the profile of the pothole and corrugations were caused by wear on the concrete surface as well as deviations in the actual profile during construction of the potholes.

The results obtained with the profiling of the Can-Can Machine indicated that the Can-Can Machine can profile a terrain with an accuracy in the order of 5 mm.

5. Profiling 3-Dimensional rough road

The Gerotek Test Facilities was established to satisfy an urgent need for an all-encompassing test facility at which vehicle design and development could be monitored in a typical South African environment (Gerotek, 2007). This first class test facility offers unique heat and altitude test conditions. Figure 66 shows an aerial photograph of Gerotek (Google Earth, 2007).



Figure 66: Gerotek Test Facility (Google Earth, 2007).

The tracks on the Suspension track at Gerotek are used to perform repeatable and comparative suspension tests under simulated conditions. These tracks are used to test the body structure, body mountings, suspension, axles, steering, chassis, driveline durability and ride comfort. The parallel corrugations, angled corrugations and potholes on the Gerotek suspension track were profiled in paragraph 4, where the ability of the Can-Can Machine to profile simple obstacles was investigated. In this paragraph, profiling of 3-dimensional rough roads is performed.

The Belgian paving on the suspension track was profiled using all three methods proposed in paragraph 3. The fatigue track, Ride and Handling track as well as the rough track was profiled using only the Can-Can Machine due to the time consuming nature of the Photogrammetry and Laser scanner methods which make them unfeasible for profiling large sections of terrain.

5.1. *Suspension Track - Belgian Paving*

The Belgian paving is mainly used for testing ride comfort and durability of a vehicle. Figure 67 shows the Belgian paving at the Gerotek Test Facility. The Belgian paving was profiled with the Can-Can Machine, Photogrammetry and the Laser Scanner. The profiles obtained with the three methods are compared with each other by comparing the Displacement Spectral Densities.



Figure 67: Belgian paving at Gerotek.

5.1.1. Can-Can Machine

The Can-Can Machine was the first profilometer used to profile the full 100 m of the Belgian paving. The profile of the terrain is available as soon as the data is downloaded from the data acquisition system and run in a pre-written Matlab program. Figure 68 shows the Can-Can Machine in the process of profiling the Belgian paving. A section of the profile is shown in Figure 69. This is an excellent representation of the Belgian paving in colour. The Belgian paving was profiled with an accuracy of better than 5 mm and the Displacement Spectral Density of the profile is calculated, compared and examined in paragraph 5.5.

The Can-Can Machine profiled the Belgian paving at a speed of 0.98 km/h. The full 100 m of the Belgian paving was profiled in 12 minutes and the data reduction only required a few minutes.



Figure 68: Can-Can Machine profiling Belgian paving.

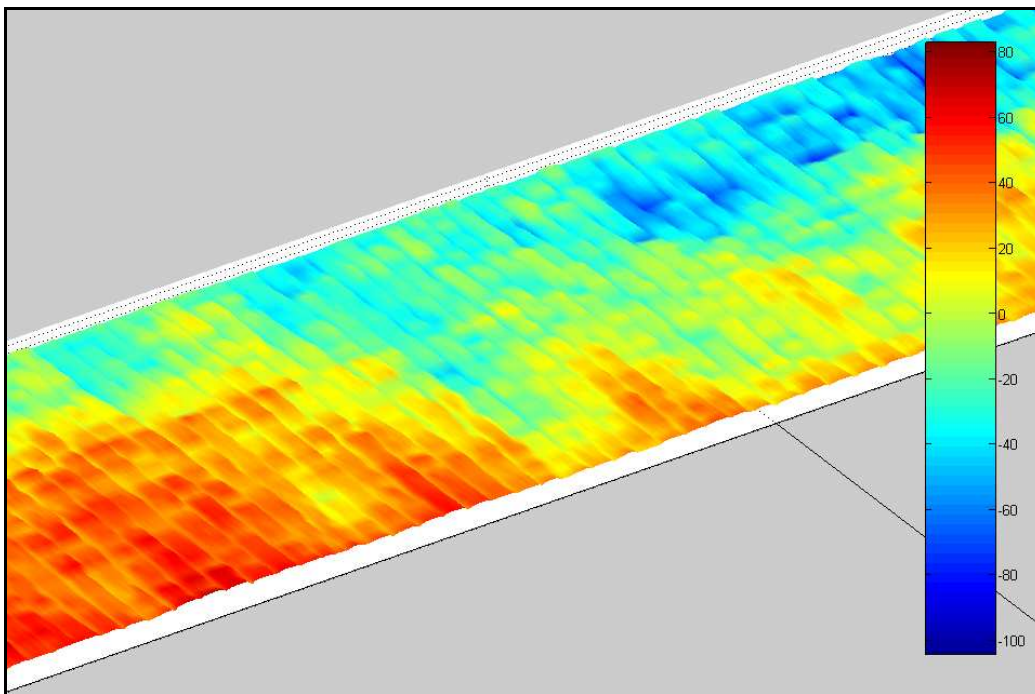


Figure 69: Can-Can profile of Belgian paving.

5.1.2. Photogrammetry

A Pentax K10D Digital camera with a PH-RBA 18-55 mm lens was used to photograph the Belgian paving. The Pentax K10D Digital camera has a stabilized ten mega pixel CCD. The PH-RBA 18-55 mm lens has an angle of view of 76 degrees at 18 mm and the focus distance was locked at the widest angle of view at 18 mm.

The photographs of the Belgian paving were taken with the use of a purposely build tripod with 6m long legs (see Figure 70). The tripod elevated the digital camera to a height of 4 m. With the camera positioned at 4 meters above the ground it was possible to capture the entire 4 m width of the Belgian paving. A 50 m section of the Belgian paving was profiled with the use of photogrammetry.



Figure 70: Tripod used to capture photographs.

The calibration certificate of the Pentax K10 camera is given in Appendix A. Figure 71 gives an example of the photographs used in the photogrammetry. The white squares in the photograph are the surveyed control points as described in paragraph 3.2.2.



Figure 71: Sample photograph used for photogrammetry.

Photographs of the 50 m section of the Belgian paving were captured with a 60 % overlap, after the control points were surveyed. The procedure as described in paragraph 3.2 was completed and a profile of the Belgian paving was produced. Figure 72 is a graphical representation of the Belgian paving as profiled with Photogrammetry. This profiling method has 3 mm accuracy but requires a great deal of time and funding to produce when compared with the Can-Can Machine. Figure 73 shows the Belgian paving profiled with Photogrammetry as plotted in Matlab.

Profiling a 50 m section of the Belgian paving with the use of the Photogrammetric method required 15 min/m to survey the control points and to capture the photographs. The mapping and processing of the photographs required in the order of 8 hours/m². This required time scale to profile 1 m² of terrain made the photogrammetric profiling method unfeasible to profile large sections of a terrain.

More terrain detail is apparent in Figure 72 and Figure 73 if compared with the profile obtained with the Can-Can Machine in Figure 69. A curvature effect on the individual photographed models can be seen on the 3-D model generated with Photogrammetry in Figure 72. This was a direct effect of an inconsistent lens calibration. It is also normal to get some distortion with the very wide angle lens (18 mm) used.

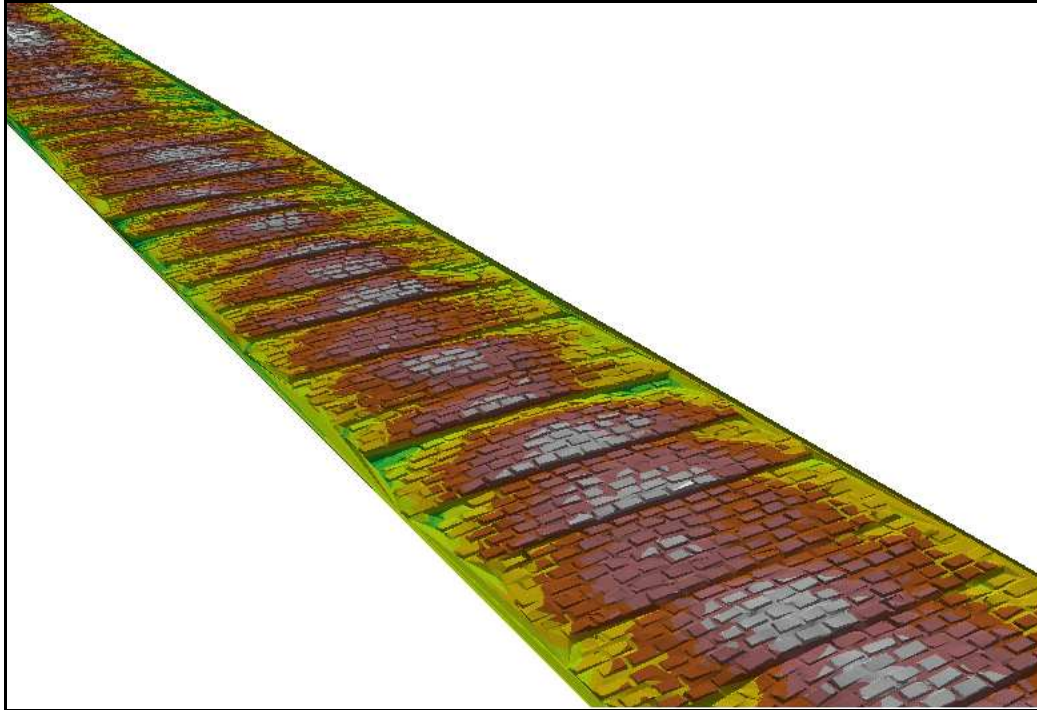


Figure 72: Belgian paving profile from Photogrammetry.

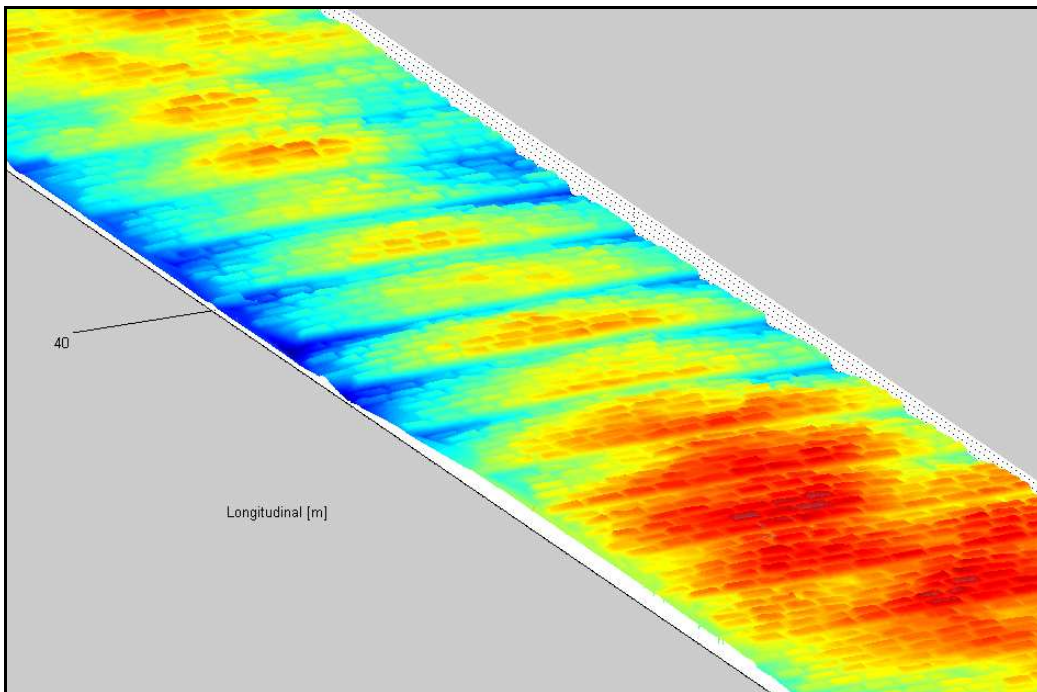


Figure 73: Belgian paving profile from Photogrammetry, plotted with Matlab.

The camera used to photograph the Belgian paving was a Pentax K10D Digital Camera with a standard 18-55 mm zoom lens locked in the 18 mm zoom setting. Off-the-shelf cameras are fitted with mass produced wide angle lenses in which the distortion is not significantly small enough for a photogrammetric application. The molds used to shape the mass production lenses are only calibrated at intervals of approximately 10 000 lenses produced. On photogrammetric assignments in practice, a professional medium format camera is used, these camera lenses are produced with minimum distortion and every lens is tested for inconsistencies. Every time a lens is made the lens mold is calibrated for optimum radial results. The medium format camera lens can be calibrated and the distortions are small enough to apply in a photogrammetric project. The radial distortion graphs in Figure 74 and Figure 75 show the different distortion results of the above mentioned lenses.

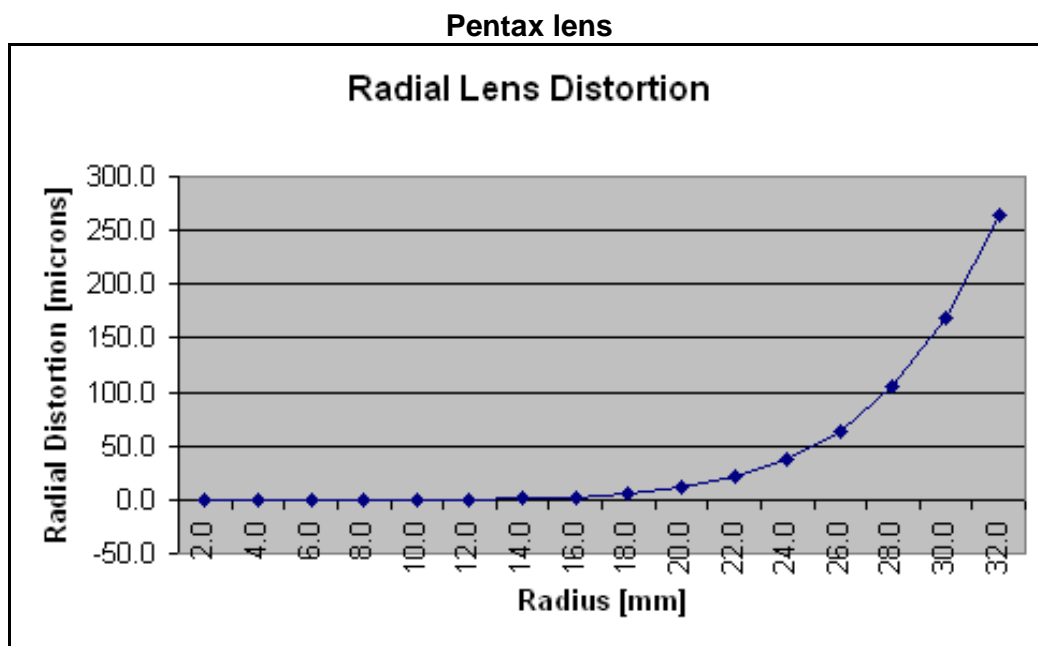


Figure 74: Lens distortion of the Pentax lens.

The Pentax lens yielded a distortion of up to 270 microns at the edge of the lens. In comparison the Hasselblad lens yielded a distortion of only 1.1 microns at the edge of the lens. The dome effect on the final 3-D model for the Belgian paving profiled with Photogrammetry was thus a direct result of this distortion in the lens. The distortions in the lens were exaggerated with the use of the colour representation in Figure 72 and Figure 73.

This project could not be executed with a Hasselblad camera since the lens used on the Hasselblad camera was a fixed lens with a longer focal length. A minimum of 8 meters was required between the lens and the target for optimal results. In addition the longer focal length on the Hasselblad camera reduces the distortion in the lens.

Medium format Hasselblad lens

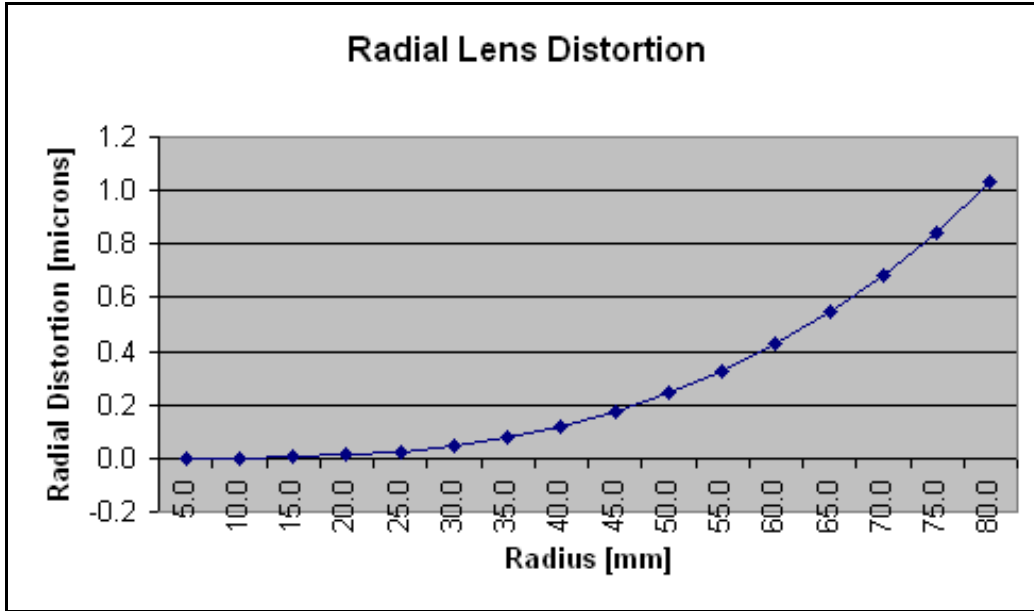


Figure 75: Lens distortions of the medium format Hasselblad lens.

It has been documented that some off-the-shelf 35 mm base digital cameras have been successfully calibrated to meet photogrammetric standards. The calibration software applied for this result was still in a development phase and not available in South Africa (Swart 2008).

The Displacement Spectral Density of the profile is calculated, compared and examined in paragraph 5.5.

5.1.3. Laser scanner

The Laser Scanner was also used for profiling a 40 m section of the Belgian paving. The profiled section was only 40 m due to bad weather on the night of profiling. The profiling proceeded at night due to the laser’s ability of only measuring on a concrete surface at night. A 10 second long-exposure photograph shown in Figure 76 shows the set-up and operation of the Laser Scanner.



Figure 76: Laser scanner in operation on the Belgian paving at night.

The Laser Scanner can only profile a 2,4 x 2,4 m square at a time, thus the following procedure is performed to profile a 40 m section of the Belgian paving. The three points on the corners of the profiled square, measured at the beginning of the profiling procedure, was marked and surveyed in a local coordinate system. The following profiled square, which was next to the previous square, was profiled with the three measured starting points in line with the previous square. This was done sequentially and was used to place all of the profiled squares in sequence.

The profiled squares were added together and plotted in Matlab. Figure 77 shows the Laser Scanner profile of the Belgian paving.

The Laser Scanner profiles at 8 m/hour and requires in the order of 1 min/m for the processing of the measured data.

The resolution of the Laser Scanner profiled Belgian paving is lower when compared to the Can-Can and Photogrammetry profiles. This is due to the larger mesh size of the Laser Scanner profile. The comparison of the Displacement Spectral Densities will provide a good indication on the effect the mesh size has on the frequencies generated by the Belgian paving. The Displacement Spectral Densities are calculated and compared to the profiles of the Can-Can and Photogrammetry profilometers in paragraph 5.5.

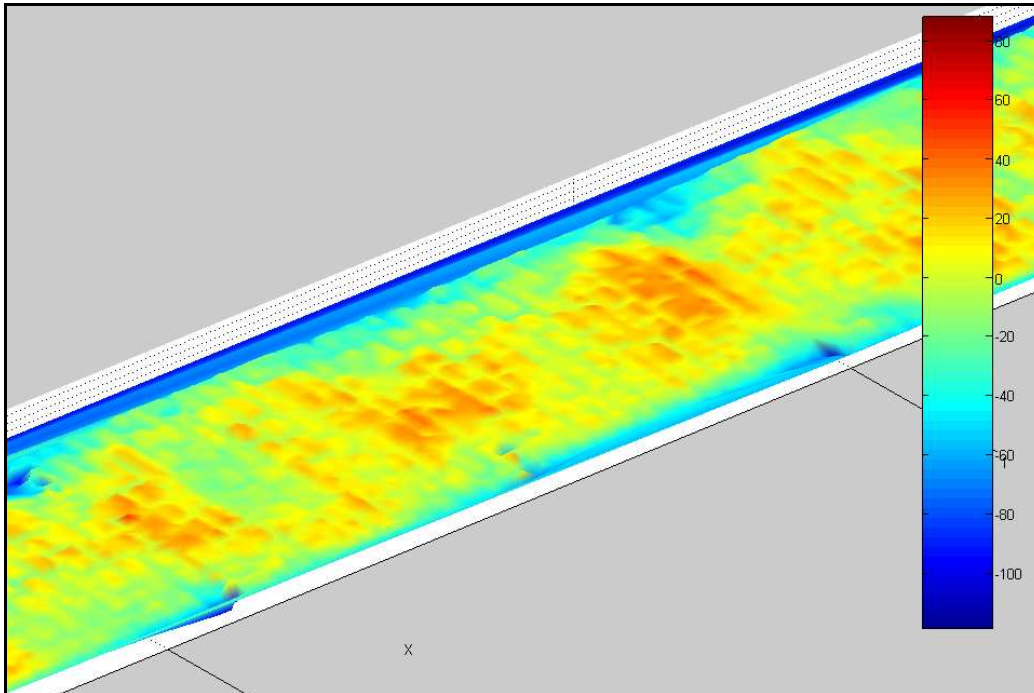


Figure 77: Laser Scanner profile of Belgian paving.

5.2. *Fatigue track*

The Fatigue section on the Suspension track at Gerotek accelerates the fatigue life of a vehicle's suspension by performing repeatable and comparative suspension tests under simulated conditions. The Fatigue track may appear smoother; however the RMS value of the Fatigue track is higher than the RMS value of the Belgian paving. Thus the Fatigue track tests the durability of the vehicle's suspension. The Can-Can Machine profiling the Fatigue track at Gerotek is shown in Figure 78. A full length 3-D profile of the Fatigue track was profiled and as a result a 3 x 100 m profile was obtained. A section of the Can-Can profile of the Fatigue track is shown in Figure 79.



Figure 78: The Can-Can Machine profiling the Fatigue track.

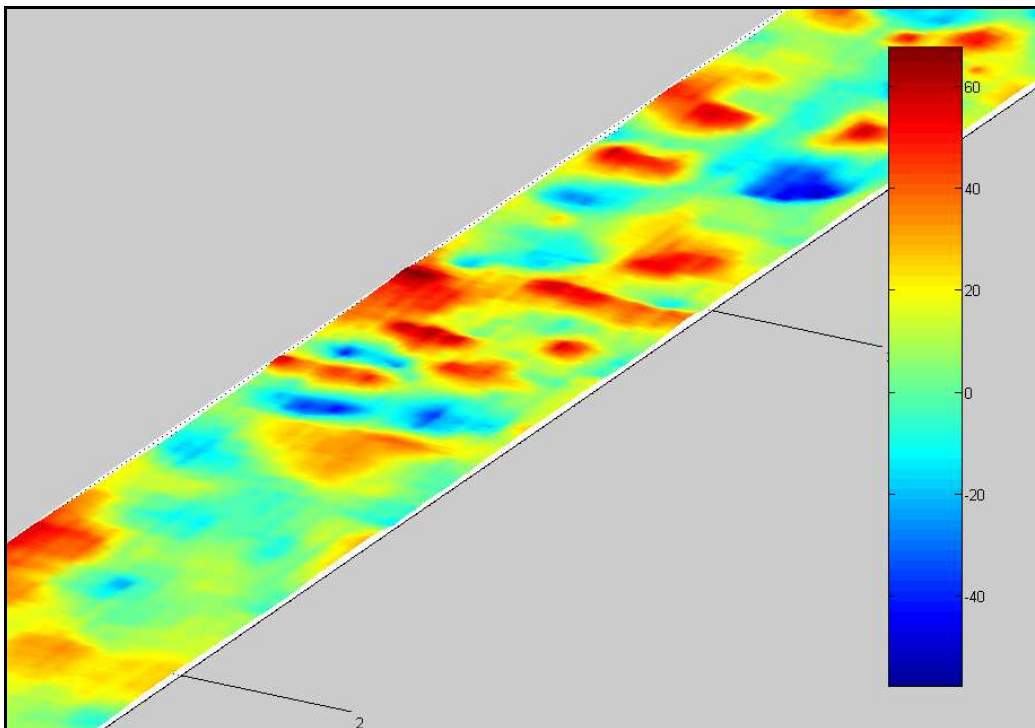


Figure 79: Can-Can profile of the Fatigue track.

The Displacement Spectral Density of the Fatigue track is calculated, compared and examined in paragraph 5.5.

5.3. Ride and Handling track

The Ride and Handling track at Gerotek is 4.2 km in length and is used for testing the ride comfort, driveline endurance and handling characteristics of a vehicle. The track consists of up and down hills, constant radius and decreasing radius turns, positive camber and negative camber corners and low speed as well as high speed corners. In addition the track also includes sections for low mobility vehicles and high mobility vehicles. For the purpose of this study only the low mobility vehicle sections were profiled with the use of the Can-Can Machine. This was done due to the fact that the high mobility vehicles sections were used only for large military vehicles. Figure 80 shows an aerial photograph of the Ride and Handling track with the Can-Can Machine profiled section in green. The surface of the Ride and Handling track is transversely tined concrete (see Figure 81).

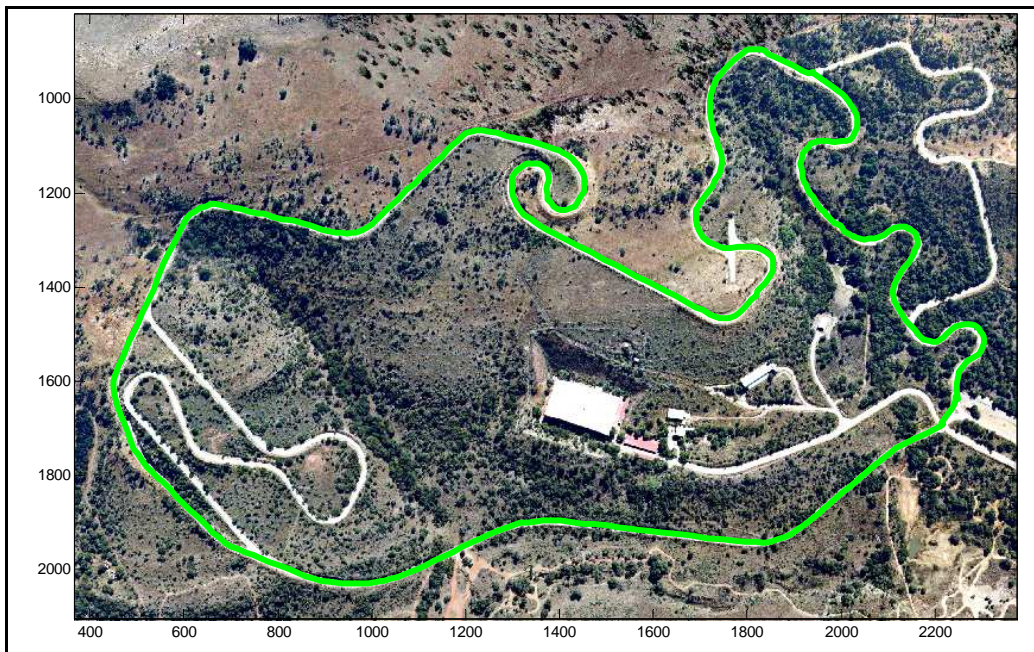


Figure 80: The profiled section of the Ride and Handling track at Gerotek.

The Ride and Handling track was profiled with the Can-Can Machine by marking control points on the concrete terrain with a spray can at 10 m intervals. The spray can was triggered with a trigger mechanism which was built in-house. The trigger mechanism used a 12 volt SANJI central locking actuator which presses on a trigger which in turn allows the spray can to release paint onto the terrain. The trigger mechanism is shown in Figure 81.

Pro Mapping cc surveyed the control points with a DGPS and was used in placing the profile recorded by the Can-Can Machine in a global coordinate system. A spline was fitted through the surveyed control points and the Rodrigues' rotation formula (Rodrigues' rotation formula 2008) was applied in

orientating the profile of the track with the spline. This gave the global position and orientation of the Can-Can Machine frame on which the profile measured by the arms could be superimposed after correction using the tilt sensor data. An exceptional 3-D profile of the Ride and Handling track was generated with this method. The Can-Can profiled Ride and Handling track is shown in Figure 82 and Figure 83.

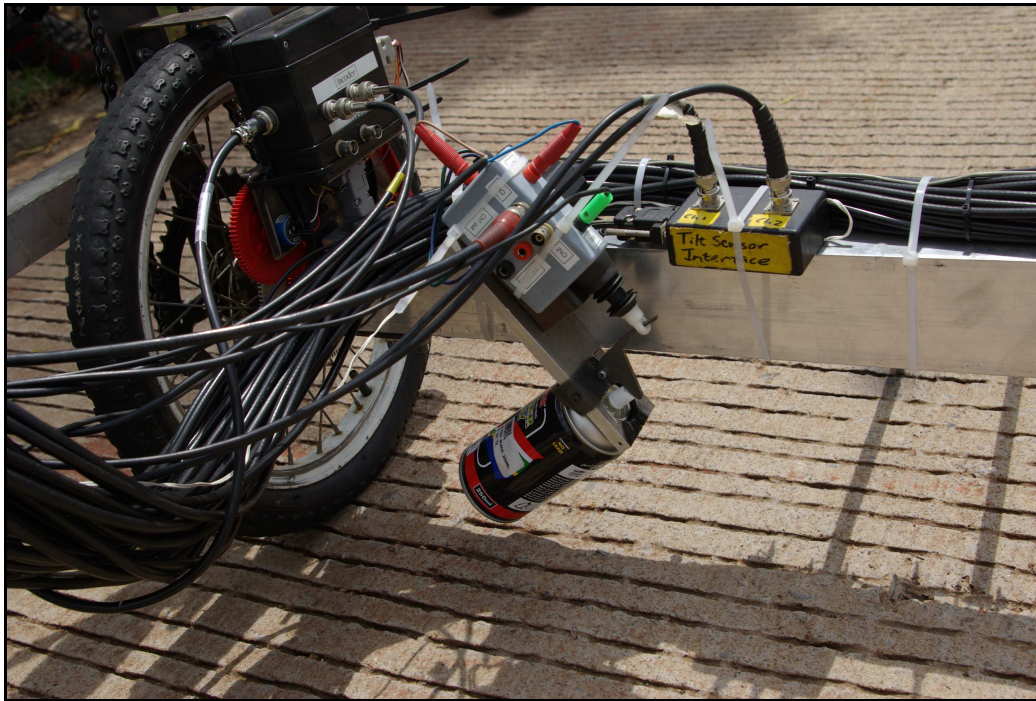


Figure 81: Trigger mechanism on Can-Can Machine.

The concrete surface of the Ride and Handling track appears smooth on the close-up of the profile shown in Figure 83. This is due to the fact that the concrete surface is fairly smooth, as shown in Figure 81 and also because the colour interpolation in the profile was done over the complete vertical displacement of the profiled terrain. The total vertical displacement on the profile was 60 m, thus the colour's resolution was not sensitive enough to detect a 10 – 20 mm change in height on the profile. Figure 84 is a close-up of a section the Ride and Handling track's profile with the colour interpolation performed over the close-up section.

The result of the profiled Ride and Handling track was very representative of the actual Ride and Handling track. A lot of detail was captured in the profile and the profile proved that the Can-Can Machine was capable of profiling a 4.2 km section of a terrain relatively quickly.

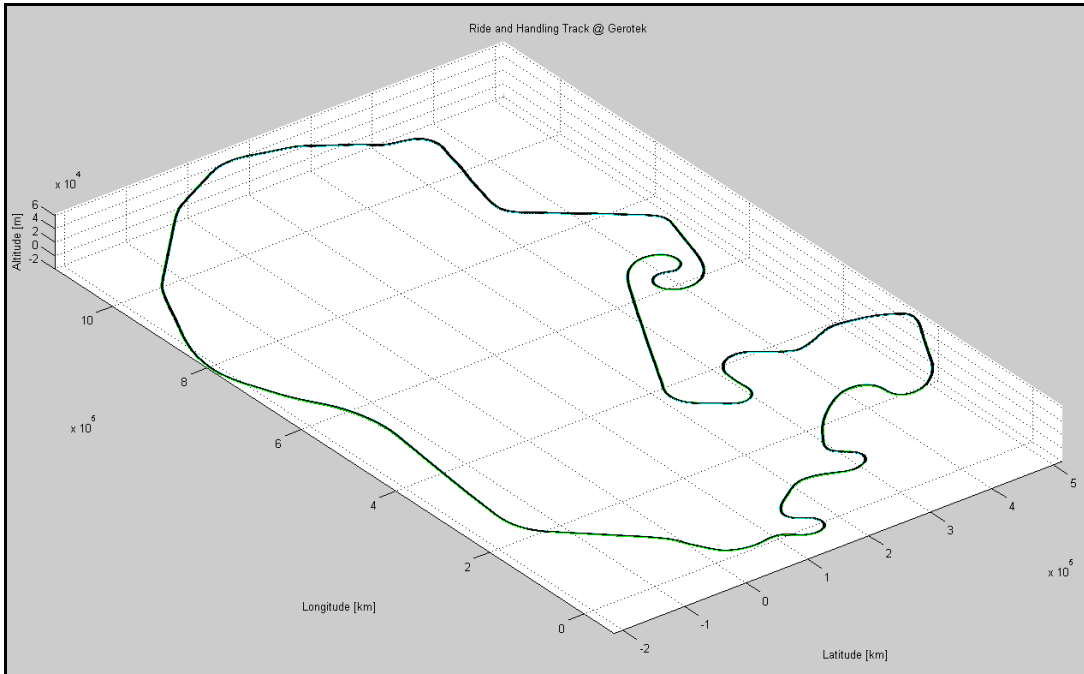


Figure 82: Ride and Handling track profiled with Can-Can Machine.

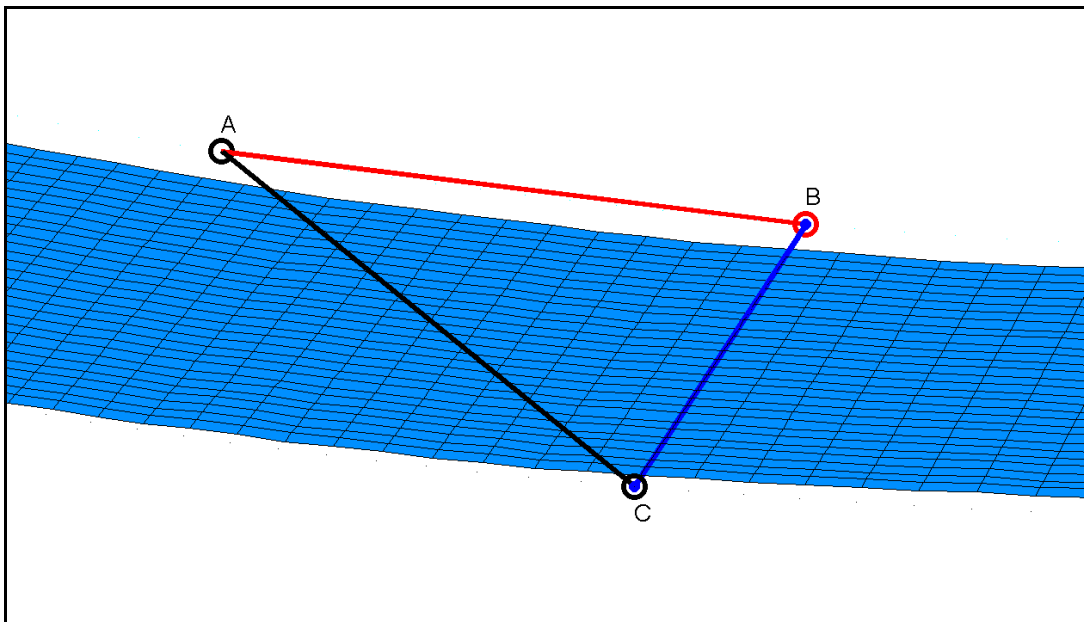


Figure 83: Close-up of Ride and Handling track with model Can-Can Machine.

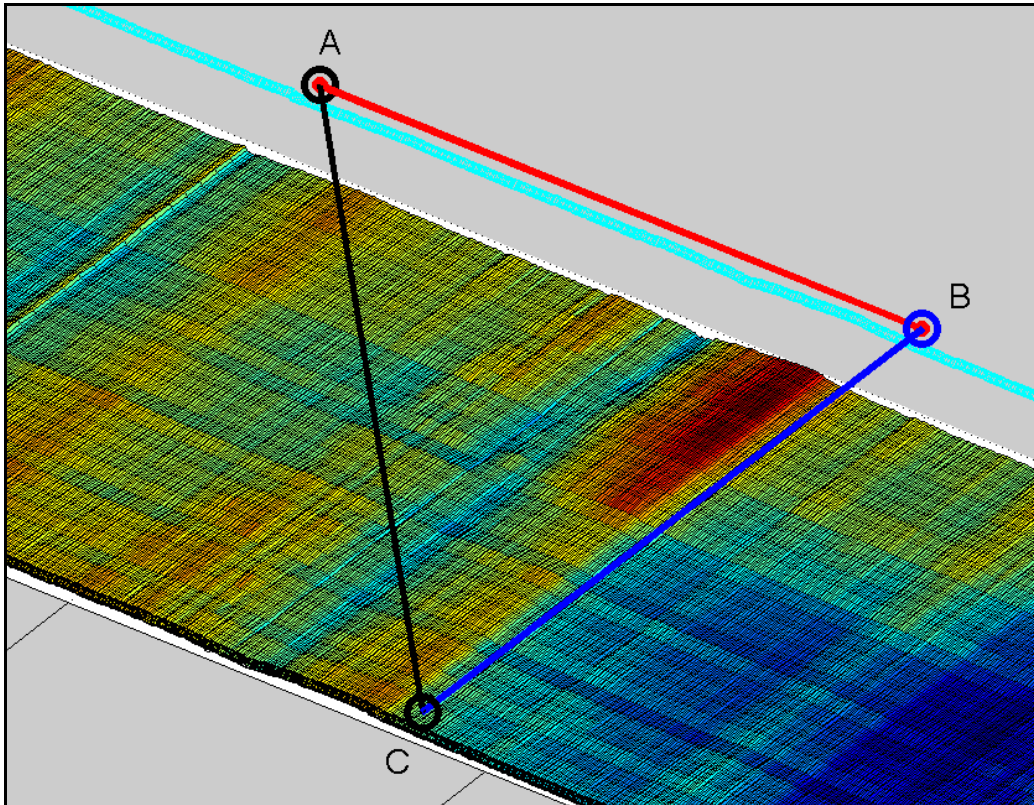


Figure 84: Close-up of the Ride and Handling track profile.

The Ride and Handling track was profiled at 0.98 km/h and the data processing required was 500 m/hour which was more time required than previous Can-Can profiled terrains due to the length of the Ride and Handling track.

The Displacement Spectral Density of the Ride and Handling track is calculated, compared and examined in paragraph 5.5.

5.4. *Rough track*

The Rough track at Gerotek is used for evaluating the rough terrain mobility and structural endurance of all-terrain vehicles. The track tests vehicle durability under accelerated conditions, including: chassis, body, suspension, steering, axles, differential locks, mountings, etc. Relative movement between body and cabin, chassis and wheels are also evaluated together with ride comfort and interior noise levels. The layout and surface varies with hills, ditches, chassis twistors, bumps and rocks all embedded in concrete to maintain a permanent profile. The concrete surface is fairly coarse to provide sufficient traction. The track is extremely rough and vehicle speeds above 20 km/h are seldom achieved.

For the purpose of this study an 800 m section of the track was profiled. This is a section of the track most frequently used for ride comfort assessment on extreme terrains. The profiled section is shown in Figure 85.

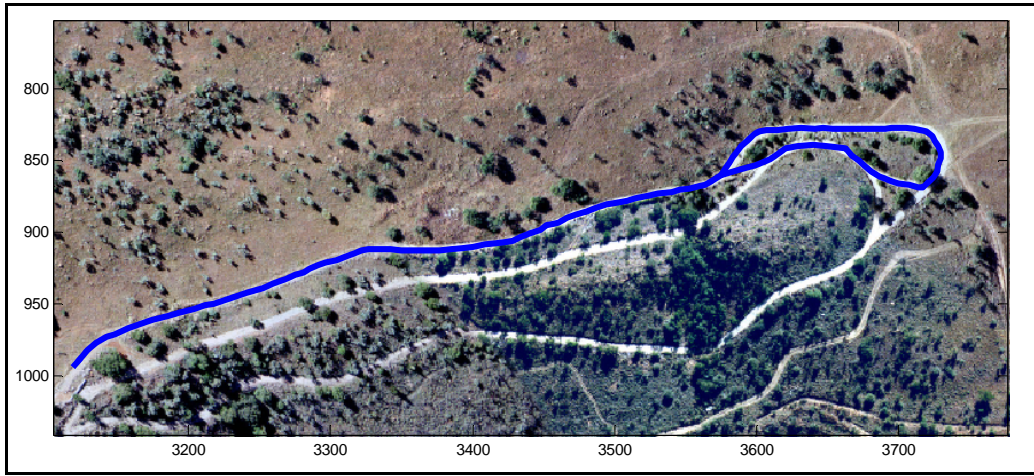


Figure 85: Profiled section of Rough track.

Tests completed, with the Can-Can Machine moving over large obstacles while profiling, indicated that the structural stiffness of the profilometer was too low for the profiling of the Rough track and will affect the accuracy of the Can-Can Machine. The low structural stiffness was due to the size of the profilometer and the requirement for the profilometer's weight to be as low as possible.

To reduce the vertical movement and input to the structure of the Can-Can Machine, a 9 m long mobile track was manufactured from lip channel. One side of the Can-Can Machine runs on a mobile track when profiling the Rough track at Gerotek. The side of the Can-Can Machine running on the mobile track was the driver wheel and the front wheel used for steering. Guides were made that guided the wheels on the beam and prevented them from falling off the beams. The mobile track supplied the Can-Can Machine with a straight line reference between surveyed points which simplified processing the profile of the Rough track. This mobile track consisted of two 4.5 m lip channel beams, each placed on three scissor jacks. The scissor jacks were used to stabilize the beams and adjust the height in order to maintain the horizontal reference set for the rear beam of the Can-Can Machine. This simplified the movement of the Can-Can Machine over the very rough terrain due to the fact that only one wheel of the profilometer was in direct contact with the terrain.

The beams were placed end-on-end with one another on the edge of the Rough track (to follow the course of the Rough track) and the Can-Can Machine started on one beam and moved along the beam onto the following beam, after which the rear beam was placed in front of the beam on which the Can-Can Machine was moving. This procedure was followed for the length of the profiled terrain (see Figure 87).

The front point of each beam had a reflective target that was surveyed with a total station at each placement of the beam as the Can-Can Machine was moving over the beams. The reflective targets on each beam also triggered a retro reflective optical speed sensor (Turck-Banner QS18VP6LP) that recorded the position of each surveyed point in the data file. The optical sensor was mounted next to the driver wheel which enabled it to be triggered by the reflective targets on the beams.

As with the profiling of the Ride and Handling track, the surveyed points were used in generating a spline which was placed in a global coordinate system. Rodrigues' rotation formula (Rodrigues' rotation formula 2008) was applied in orientating the profile of the track with the spline. The spline was linearly interpolated between the surveyed points with the correct amount of data points as required between each trigger.

Figure 86 shows a section of the Rough track and Figure 87 shows the Can-Can Machine crossing from one beam to another. Figure 88 shows the full Can-Can profiled Rough track and Figure 89 is a close up of a section of the Rough track.



Figure 86: A section of the Rough track at Gerotek.



Figure 87: Can-Can Machine crossing from one beam to another.

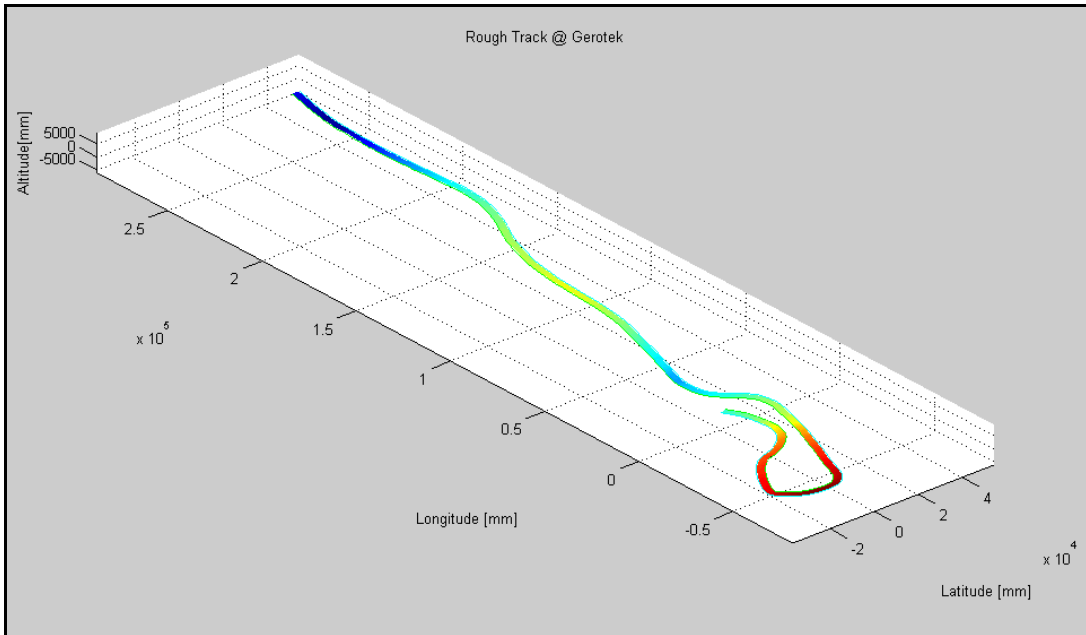


Figure 88: Profile of the Rough Track at Gerotek.

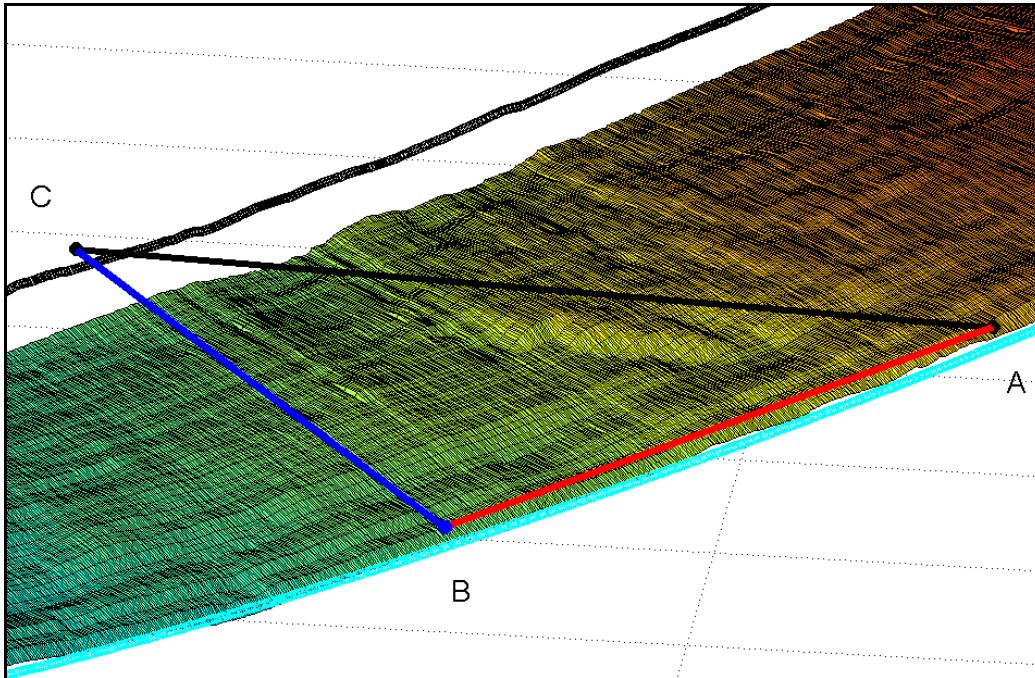


Figure 89: Close-up of the Rough track profile.

The result of the profiled Rough track was very representative of the actual Rough track. A lot of detail was captured in the profile and the profile proved that the Can-Can Machine was capable of profiling a very rough terrain in a relatively short space of time.

The Rough track was profiled at 0.1 km/h due to the roughness and profiling method used for the Rough track. The data processing required was 500 m/hour, which was more time required than previous Can-Can profiled terrains due to the length of the Rough track.

The Displacement Spectral Density of the Rough track is calculated, compared and examined in paragraph 5.5.

5.5. *Displacement Spectral Densities of profiled tracks (DSD)*

Although the main purpose of the present study is to obtain 3-D profiles of specific terrains for the use in vehicle dynamic simulations, the Displacement Spectral Density was also used to characterize the roughness of each profiled terrain. The following formula, as described in paragraph 2.8, is used for calculating the Displacement Spectral Densities.

$$S_{xx}(F) = \frac{|X_{\delta}(F)|^2}{2\Delta F}$$

The roughness of each track is compared with a class-A road to a class-H road, according to ISO 8606 road classification (ISO, 1995), which is a comparison from a smooth to a very rough terrain.

5.5.1. Belgian paving

The Displacement Spectral Density of the Belgian paving profiled with the Can-Can Machine was calculated for each arm after which the average of all 30 arms together was determined. Figure 90 shows the Displacement Spectral Densities of the Can-Can profiled Belgian paving. The green lines are the Displacement Spectral Densities from the 30 arms and the black line is the average Displacement Spectral Density of all 30 arms.

The peak at 6.066 cycles/m represents an average brick size of 164 mm where the actual average brick size was close to 130 mm. This difference in brick size is due to the shape of the bricks. The discrete obstacles profiled with the Can-Can Machine did not have 90 degree steps in them. The 90 degree direction change in a step was smoothed out by the small wheels at the end of the arms on the Can-Can Machine and resulted in a larger brick size. The correct brick size was obtained when the diameter of the small wheels was subtracted from the average brick size and resulted in a brick size of 134 mm. This is acceptable for the reason that the wheel on the actual vehicle is much larger and will not see the sharp 90 degree direction changes in the profile. The peak at 22.58 cycles/m represents the average gap size of 44 mm between the bricks.

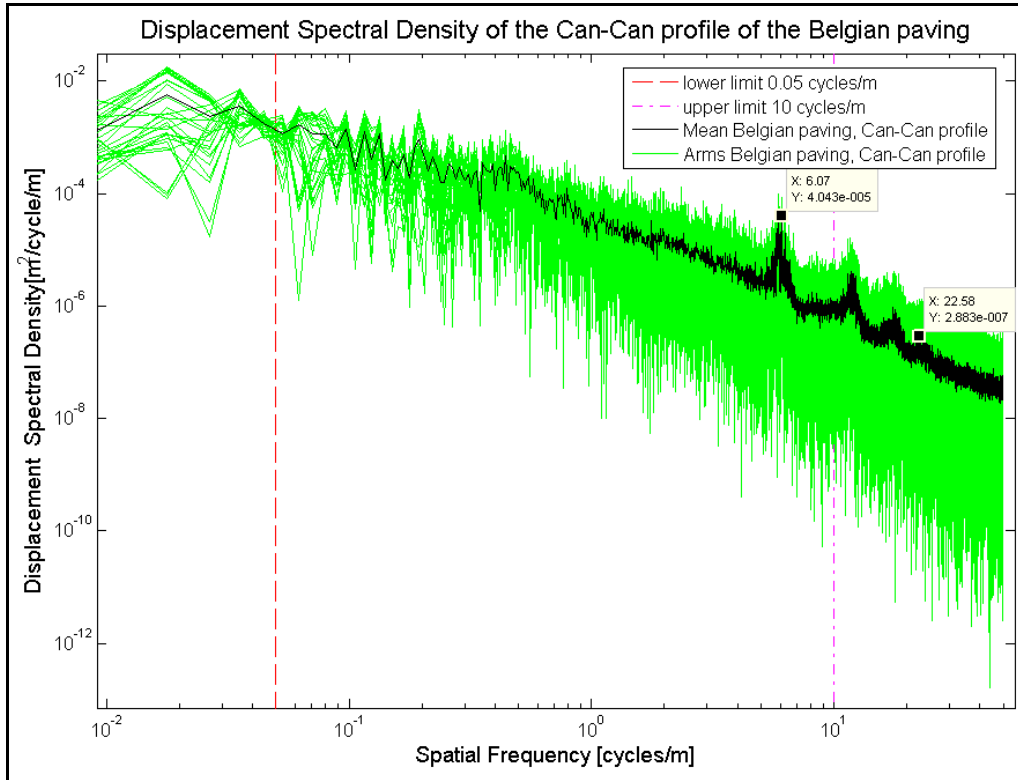


Figure 90: Displacement Spectral Density of the Can-Can profile of the Belgian paving.

The Photogrammetry profile data was determined for a 10 x 10 mm grid. The Displacement Spectral Density determined by calculating a Displacement Spectral Density for each longitudinal gridline, thus 300 Displacement Spectral Densities was calculated from the 3 x 50 m profile. Figure 91 shows the Displacement Spectral Densities of the Photogrammetry profiled Belgian paving with the blue lines each of the 300 Displacement Spectral Densities and the green line the average Displacement Spectral Density.

In Figure 91, the peak at 1 cycle/m was the result of the impurities and distortions in the lens as described in paragraph 5.1.2. This spatial frequency was evident in the Photogrammetry profile of the Belgian paving, as seen in Figure 72 and Figure 73 in paragraph 5.1.2. The average brick size is represented by the peak at 6.14 cycles/m which results in a 160 mm brick size. The larger brick size was due to the mapping procedure in which a break line around the base of the brick was mapped. The mapped break line was not always at the intersection of the brick and the ground since it was not always possible to see the intersection of the brick and the ground. A gap size of 36 mm was detected at 27.18 cycles/m and was also affected by the mapping procedure.

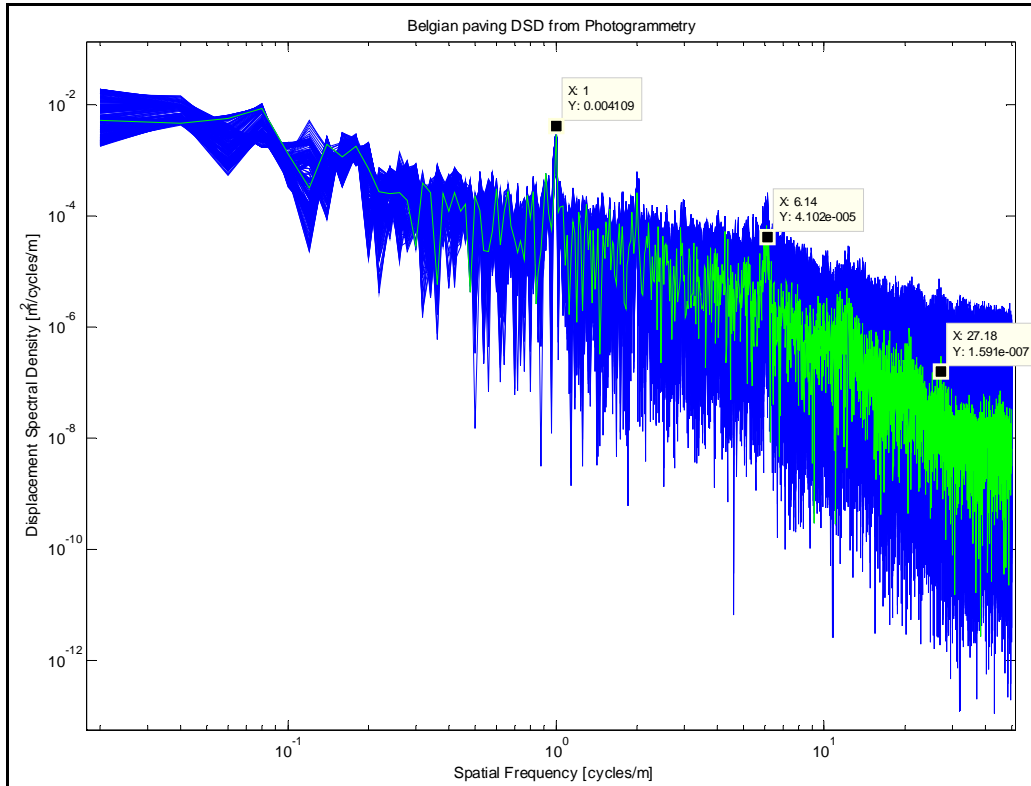


Figure 91: Belgian paving DSD from Photogrammetry profile.

Each 2,4 x 2,4 m block of the Laser Scanner resulted in a mesh with 32 perpendicular gridlines in both the longitudinal and lateral directions. The profile of a terrain profiled with the Laser Scanner was constructed as described in paragraph 5.1.3. The Displacement Spectral Density of each longitudinal gridline of the total profile as well as the average of the 32 Displacement Spectral Densities was calculated. Figure 92 shows the Displacement Spectral Density of the Laser Scanner profiled Belgian paving. The blue lines are the Displacement Spectral Densities from the 32 gridlines and the red line is the average Displacement Spectral Density of the 32 gridlines.

In Figure 92, the peak at 0.3877 cycles/m is caused by the convex shape of each individual profile as described in paragraph 3.3.1. Where as the peak seen at 4.837 cycles/m indicate that an average brick size of 206 mm are detected by the Laser Scanner. The larger recorded brick size was caused by the mesh size which was just larger than half of the actual brick size. The gaps between the bricks were not detected by the Laser Scanner due to the fact that the gaps between the bricks were smaller than the mesh size of the Laser Scanner.

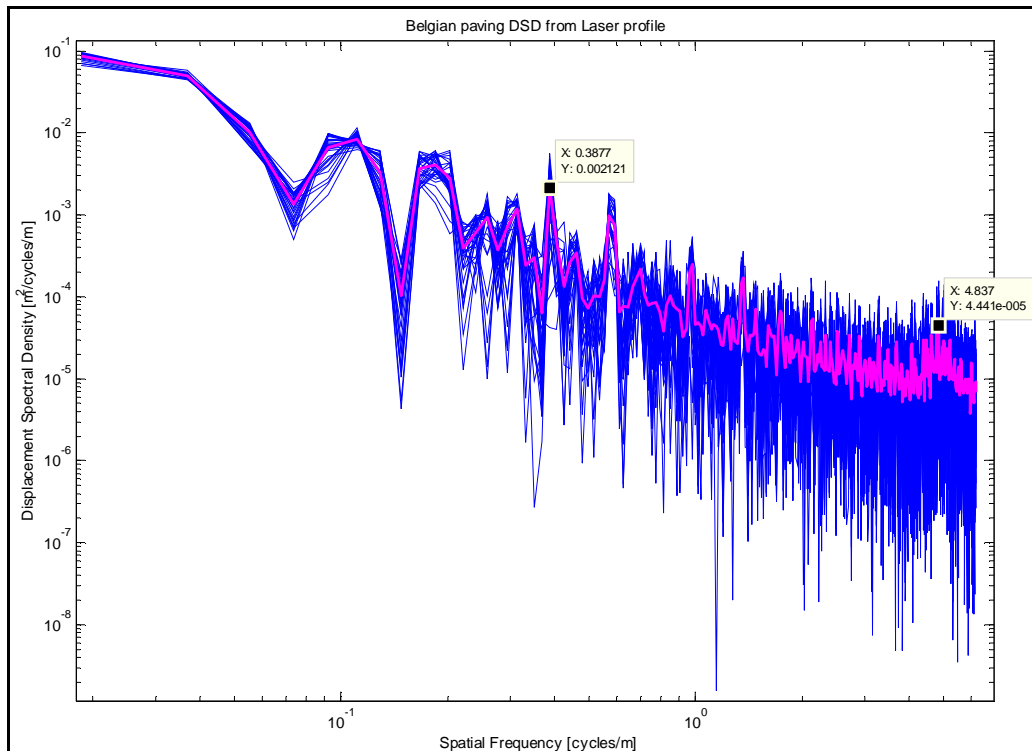


Figure 92: Displacement Spectral Density of the Belgian paving profiled with the Laser profile.

Figure 93 compares the Displacement Spectral Densities from all three profiles of the Belgian paving with Displacement Spectral Densities from class-A, class-D and class-H roads. The Displacement Spectral Densities of the class-A, D and H roads are plotted for special frequency range, 0.007 to 4 cycles/m, according to ISO 8608 (1995). The three profiling methods produced nearly equivalent Displacement Spectral Densities of the Belgian paving and indicated that the Belgian paving was a touch rougher than a class-D road. Figure 93 illustrates that the Laser profile has the lowest resolution and the Photogrammetry profile the highest resolution as expected.

From the results discussed above the following conclusions are made. The Can-Can Machine is to be used of profiling terrains due to:

- The high profiling speed and efficiency of the Can-can Machine,
- The ease of data processing,
- The accuracy of the profilometer
- And the low operating costs of the Can-Can Machine.

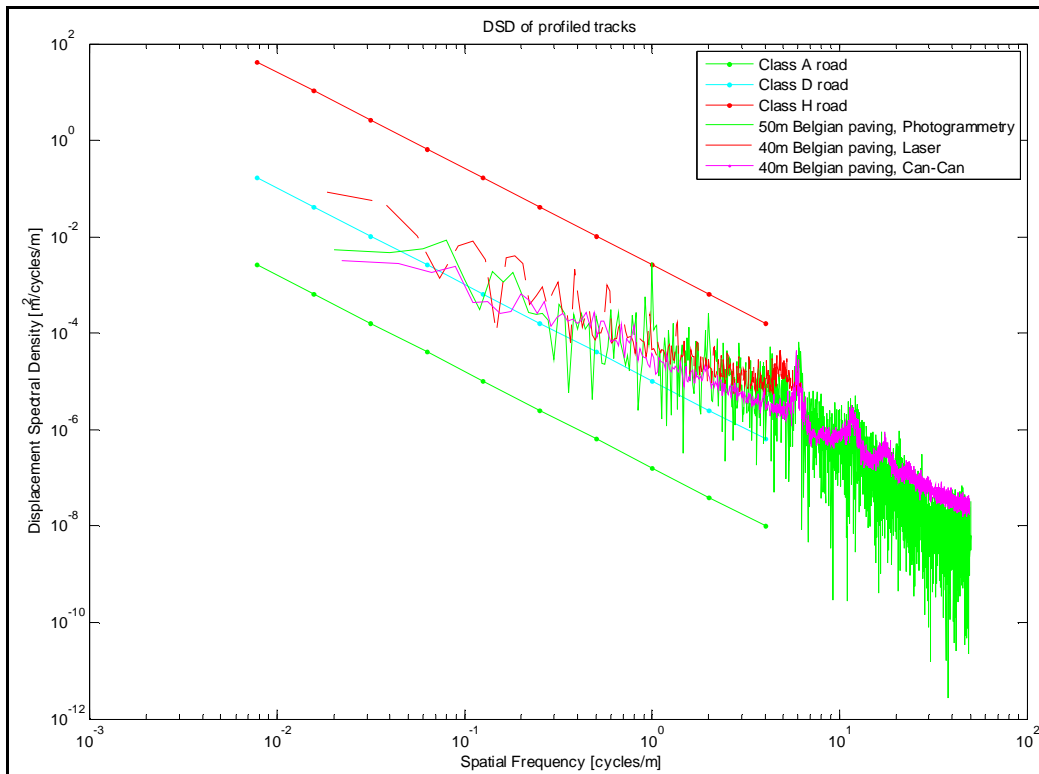


Figure 93: DSD's of all three Belgian paving profiles together with a class-A, class-D and class-H road.

5.5.2. Fatigue track

The Fatigue track was profiled only with the Can-Can Machine. The average Displacement Spectral Density in Figure 94 indicates that, compared to the class D-road, the Fatigue track generates higher amplitude inputs at spatial frequencies between 0.5 and 10 cycles/m (points A and B), but is significantly smoother below 0.5 (point A) and above 10 cycles/m (point B).

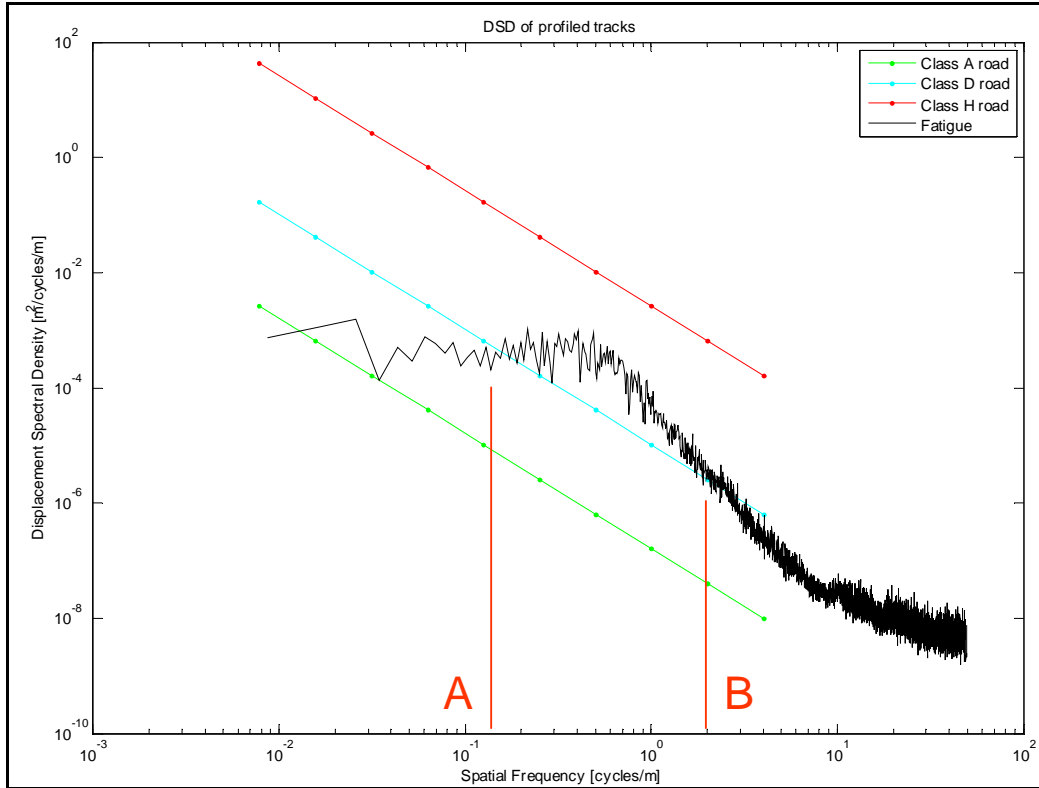


Figure 94: DSD of the fatigue track.

5.5.3. Parallel and angled corrugations

The parallel and angled corrugation track's were profiled with the Can-Can Machine and the Displacement Spectral Densities are compared to a class-A, class-D and a class-H road in Figure 95. An average distance of 760 mm between the 25 mm bumps is represented by the peak at a spatial frequency of 1.316 cycles/m. This illustrates the accuracy of the profilometer and the calculation of the Displacement Spectral Density since the actual distance between each 25 mm bump on these tracks is reported to be 750 mm. The other peaks in the Displacement Spectral Densities are fractions of the distance between the bumps.

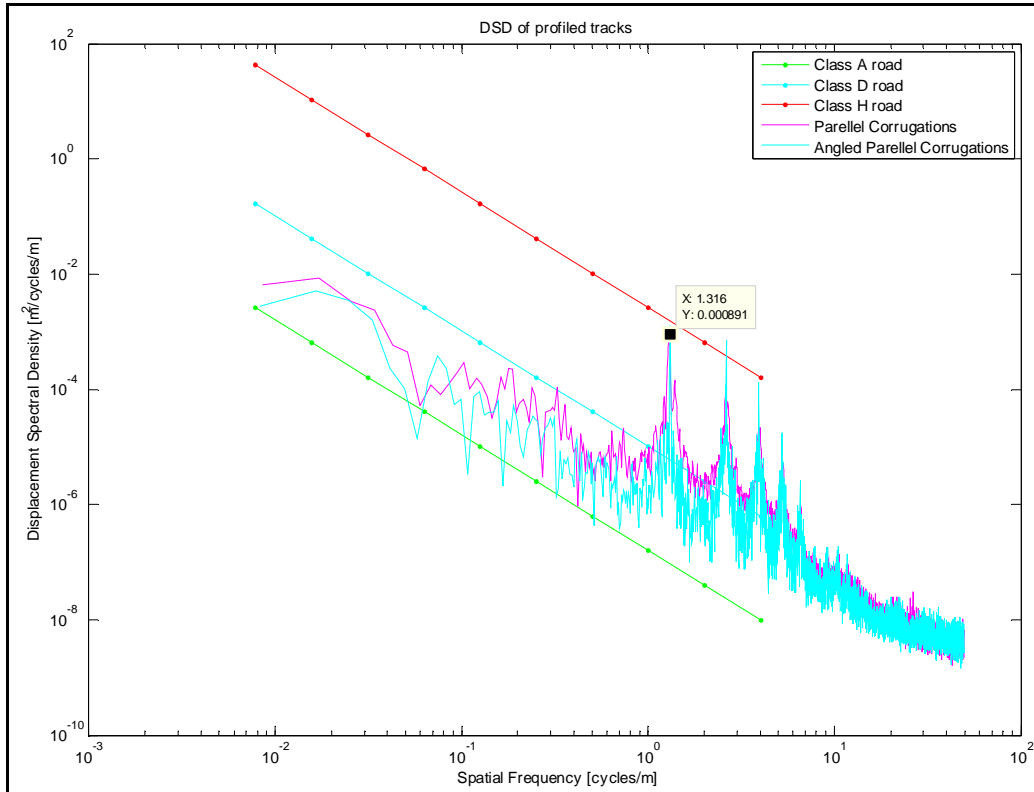


Figure 95: DSD of the parallel and angled corrugations tracks.

5.5.4. Pothole track

The Pothole track was profiled with the Can-Can Machine as described in paragraph 4.1.3. The Pothole track has 25 potholes spaced at different distances ranging from 3 m to 12 m apart and each pothole is 660 mm long at the top, 500 mm long at the bottom and 80 mm deep (see Figure 63, Figure 64 and Figure 65). The average Displacement Spectral Density of the Pothole track is presented in Figure 96. The valley at 1.782 cycles/m detects the average length of the potholes as 561 mm.

5.5.5. Ride and Handling track

The Ride and Handling track was profiled with the Can-Can Machine as described in paragraph 5.3. The Displacement Spectral Density of the Ride and Handling track, shown in Figure 97, indicates that the surface of the track is rather rough. The Displacement Spectral Density of the Ride and Handling track was calculated without the global surveyed coordinates.

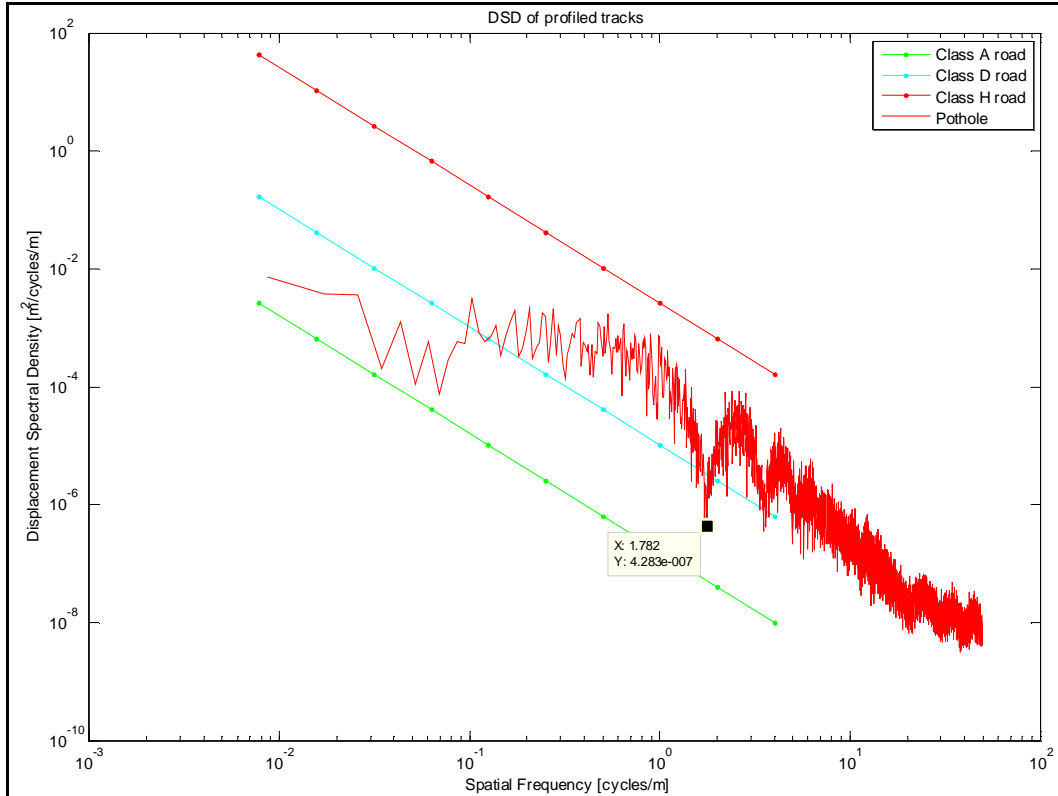


Figure 96: DSD of the pothole track.

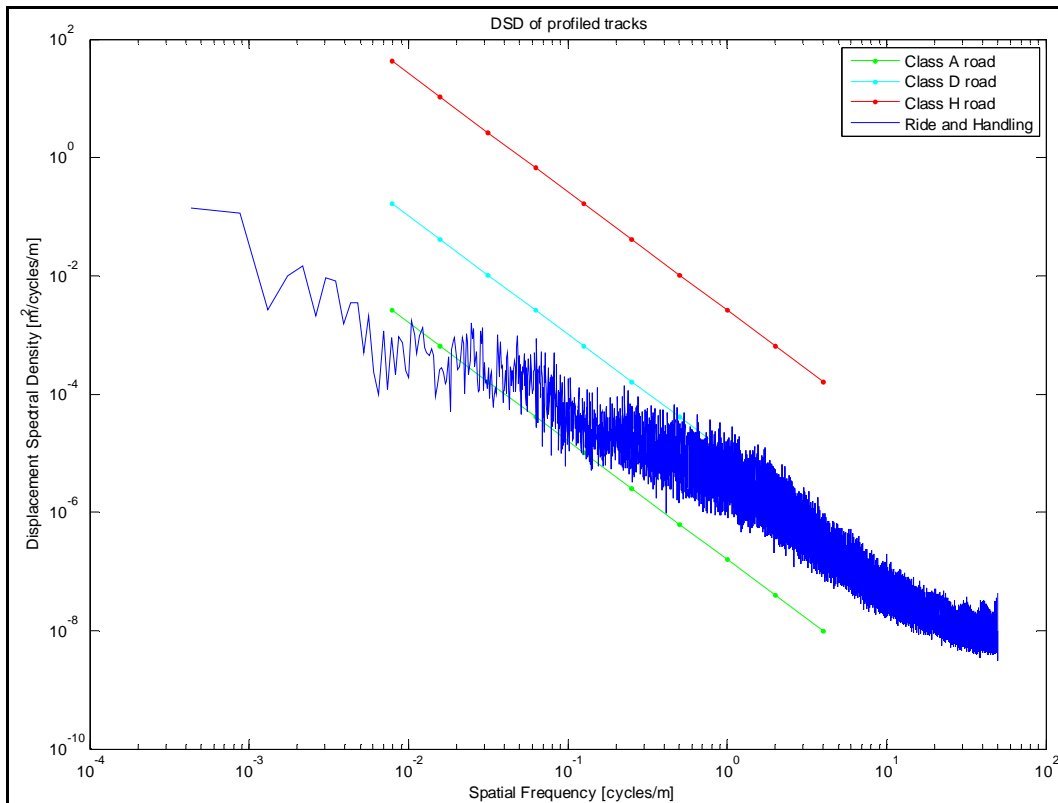


Figure 97: DSD of the Ride and Handling track.

5.5.6. Rough track

The Rough track was extremely rough and was profiled with the Can-Can Machine as described in paragraph 5.4. The Displacement Spectral Density of the Rough track is shown in Figure 98 and as expected it is classified as a class-H road. The graph also indicates that the surface roughness of the terrain was also high. This was indicated by the amplitude of the right hand side of the graph. The roughness of the terrain surface is high to increase the available traction on the terrain. Note that the log scale makes the “noise” appear smaller. The Displacement Spectral Density of the Rough track was calculated without the global surveyed coordinates.

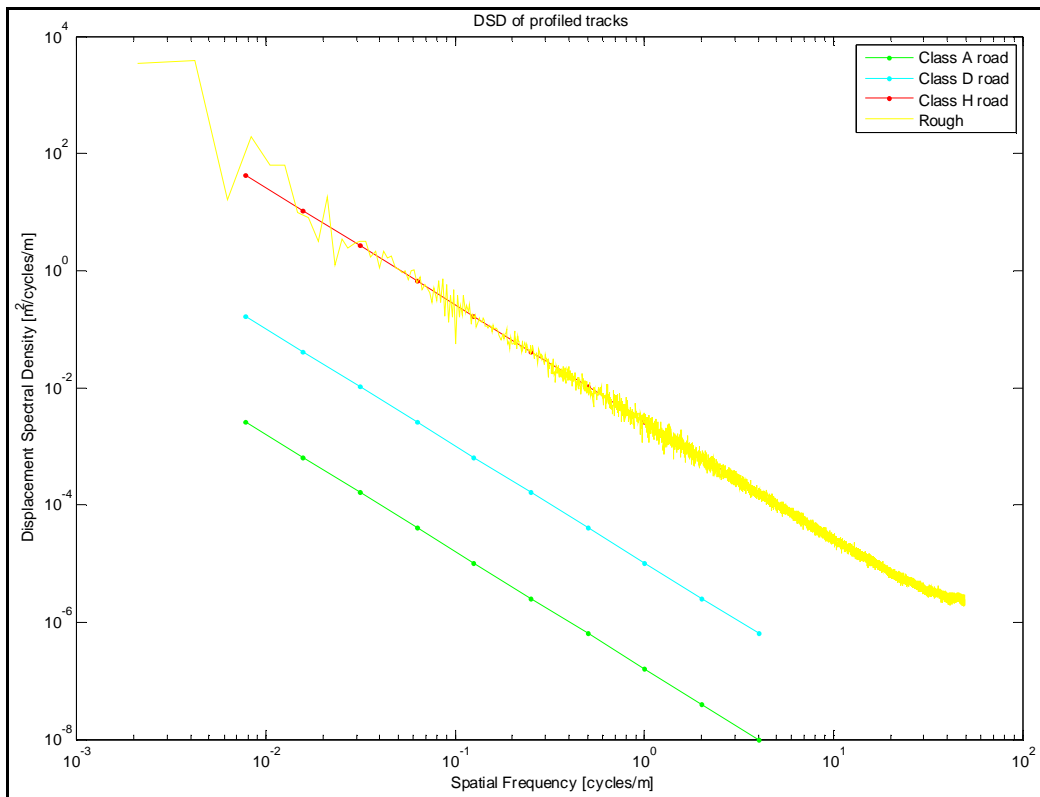


Figure 98: DSD of the Rough track.

5.5.7. Determining Roughness coefficient

The approximate linear shape of the Displacement Spectral Density when plotted on log-log coordinates is a consequence of the fact that long wavelength features in the terrain tend to have large amplitudes and short wavelengths features tend to have small amplitudes if a random terrain is

considered. The Displacement Spectral Density of a paved road surface profile normally has a more linear graph than an off-road terrain profile.

The Displacement Spectral Density is one method used in describing the roughness of a terrain. Other methods used are the route mean square (RMS) of the vertical displacement, which is equivalent to the square root of the area underneath the Displacement Spectral Density, a Power function or Inverse Power Law is often applied to DSD's of random roads using an equation of the following form:

$$S_z = A\varphi^{-n}$$

This approximation offers a very simple way of defining the characteristics of a random terrain. The terrains can only be compared to one another with the use of these methods if the same spatial frequency range is used for each terrain. For off-road profiles the reported spatial frequency range for φ should be from 0.05 cycles/m (wavelength = 20m) to 10 cycles/m (wavelength = 0.1m), ISO 8608 (1995).

The lower value of $\varphi = 0.05$ cycles/m is acceptable since the vehicle speed over off-road or rough terrain is normally much lower than the case for road. The upper spatial frequency limit of $\varphi = 10$ cycles/m is consistent with the length of the tyre contact patch, ISO 8608 (1995). Figure 99 presents an example of the Displacement Spectral Density of the Belgian paving, profiled with the Can-Can Machine, as well as an Inverse Power Law fit on the Displacement Spectral Density. The upper and lower limits of the spatial frequency window used in calculating the Inverse Power Law coefficients are also shown.

Table 2 presents results of the inverse power law approximation of each terrain, which consists of the roughness coefficient A and the road index n to describe different terrains. The first six terrains are described by Hall (1998). The roughness coefficients and road indexes of the terrains profiled with the Can-Can Machine is also presented as well as the profiles of the Belgian paving as profiled with Photogrammetry and the Laser Scanner.

This kind of approximation is not very satisfactory for most of the terrain under consideration for the present study due to the existence of definite peaks and valleys in the DSD's of most of the profiled terrains.

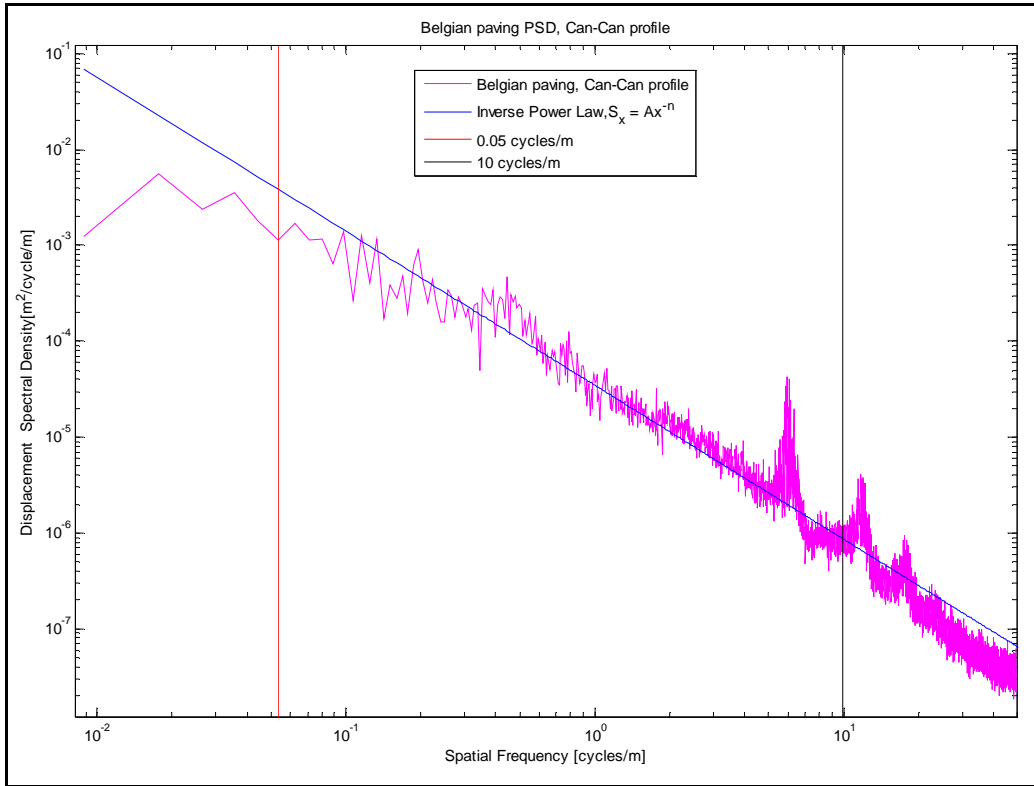


Figure 99: Inverse Power Law plot on Belgian paving.

Terrain	Roughness coefficient. A (m ² /cycles/m)	Road index, n
Smooth runway*	4.30E-11	3.8
Rough runway*	8.01E-04	2.1
Smooth highway*	4.80E-07	2.1
Highway with gravel*	4.40E-07	2.1
Pasture*	3.00E-04	1.6
Ploughed field*	6.50E-04	1.6
Belgian paving, Can-Can	3.48E-05	1.6
Belgian paving, Photogrammetry	5.72E-05	1.8
Belgian paving, Laser scanner	4.87E-05	1.0
Fatigue track, Can-Can	3.42E-05	2.9
Parallel Corrugations, Can-Can	2.20E-06	1.6
Angled Corrugations, Can-Can	7.67E-06	1.9
Pothole track, Can-Can	5.30E-05	2.2
Rough track, Can-Can	2.46E-03	1.9
Ride and Handling track, Can-Can	2.27E-06	1.8

* Hall (1998)

Table 2: Inverse Power Law values.

The roughness coefficient is the value of the Displacement Spectral Density at 1 cycle/m and the road index parameter is calculated with a spatial frequency window from 0.05 cycles/m to 10 cycles/m as indicated in Figure 99. The inverse power law approximation of each of the profiled terrains were calculated by fitting a straight line to the Displacement Spectral Density, with the use of a least squares fit and calculating the Roughness coefficient and the Road index of the straight line.

The road index of the Belgian paving profiled with the Laser Scanner is lower due to the fact that the upper limit of the spatial frequency window used in calculating the road index was used as 6.6 cycles/m and not 10 cycles/m. This was done because of the coarse resolution of the Laser Scanner profile.

The road index of the Belgian paving profiled with Photogrammetry is higher than the Can-Can Machine's due to the fact that the Photogrammetry profile had a higher resolution which contained more detail of the Belgian paving.

5.6. *International Roughness Index (IRI)*

The International Roughness Index was calculated as described in paragraph 2.9. A quarter-car model was created in Simulink which represented the Golden Car Model with the spring and damper characteristics as specified by Sayers and Karamihas (1998).

The quarter-car parameters are specified as part of the IRI statistic and the simulated travel speed is specified as 80 km/h. the Golden Car parameters are:

$$\frac{k_s}{m_s} = 63.3 \quad \frac{k_t}{m_s} = 653 \quad \frac{c}{m_s} = 6 \quad \frac{m_u}{m_s} = 0.15$$

where k_s is the spring rate, m_s is the sprung mass, k_t is the tyre spring rate, c is the damper rate and m_u is the unsprung mass.

A single 2-D line from each of the 3-D profiled terrains were used as an input to the quarter-car model for all of the profiled terrains on the Suspension track as well as the profiled section of the Rough track.

The total suspension travel, as calculated from the quarter-car model, was divided by the distance travelled in order to obtain the International Roughness Index for each specific terrain. Figure 100 shows an example of the IRI vs. the distance travelled over the Belgian paving. The IRI vs. the distance travelled plots for all of the profiled terrains are available in Appendix D.

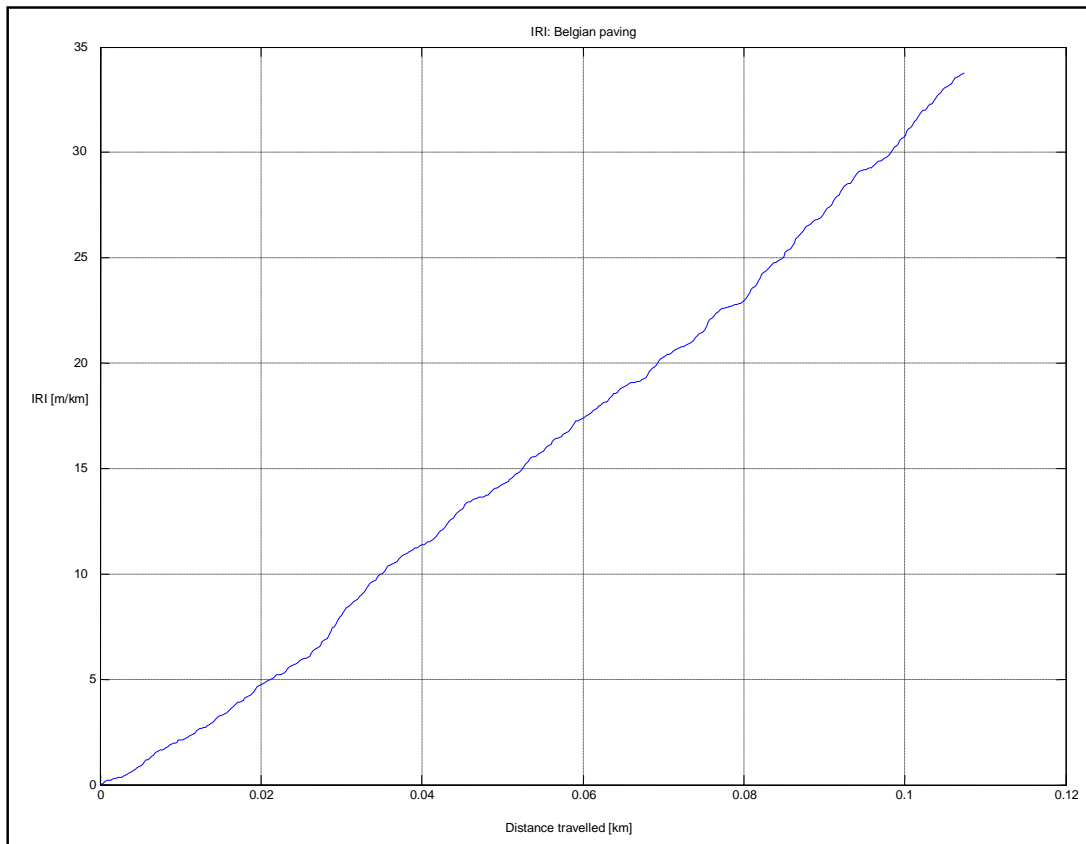


Figure 100: IRI vs. the distance travelled over the Belgian paving.

The calculated IRI for all of the profiled terrains are graphically shown in Figure 101 together with the upper and lower limits for the different road classes. Most of the roads profiled in the current study are significantly rougher than the “rough unpaved roads” presented by Sayers and Karamihas (1998).

This is an indication that the trends supplied by the International Roughness Index are only valid for smoother terrains. These smoother terrains are typically asphalt or concrete roads. This is expected as the International Roughness Index was designed for the characterization of asphalt and concrete roads. These asphalt and concrete roads are drastically smoother than the terrains which the present study concentrated on. The IRI uses a linear quarter-car model and is not compatible to the suspensions of most off-road vehicles. As a result it is recommended to use the profile of actual off-road terrains in simulations instead of statistically generated profiles.

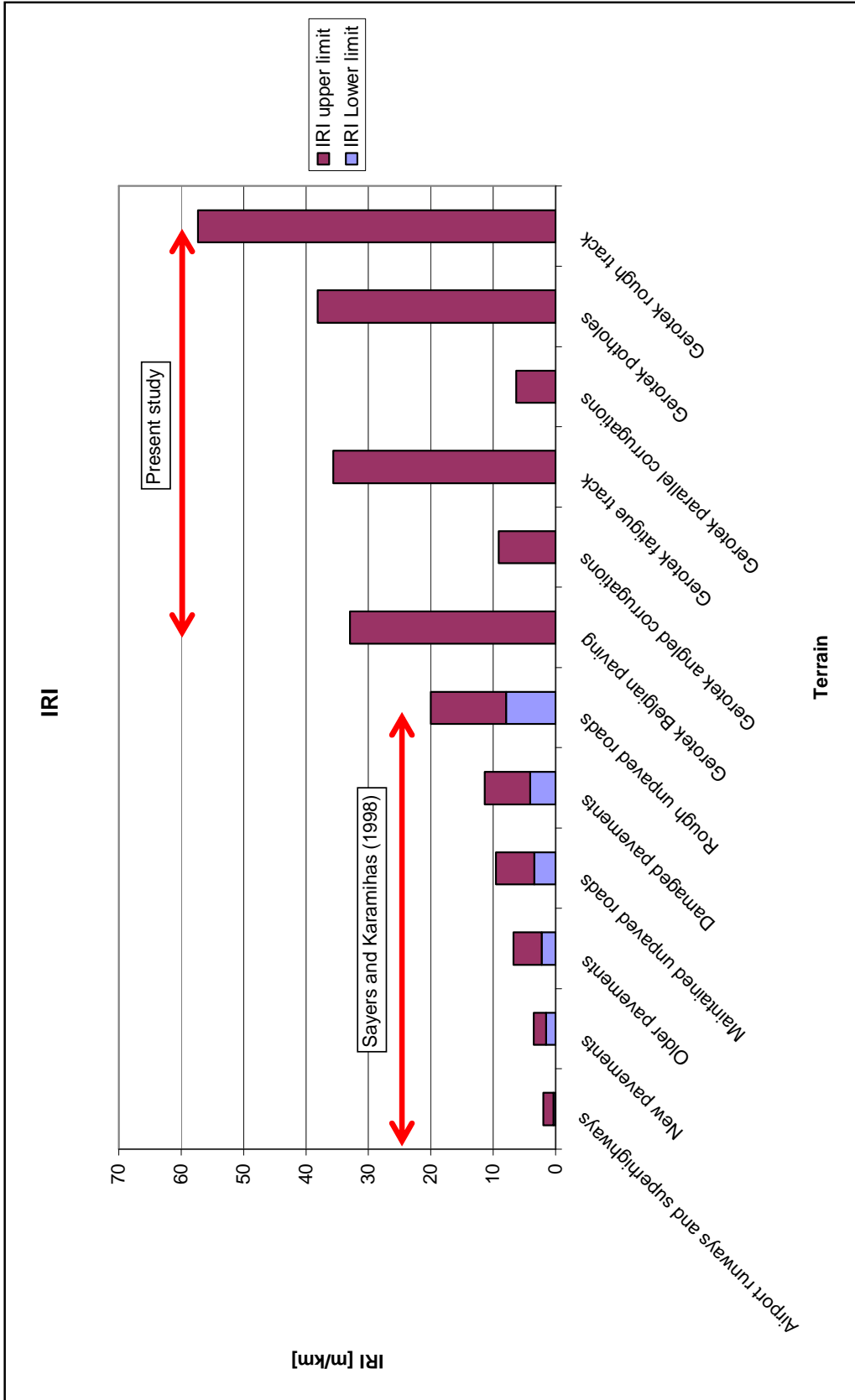


Figure 101: International Roughness Index

5.7. Summary on rough road profiling

The terrain profiles obtained with the three methods under consideration were visually very representative of the actual terrain. Although the resolution of the Laser Scanner was lower than the resolution of the Can-Can Machine and Photogrammetry a valid profile was still produced by the Laser Scanner. The resolution of the Belgian paving profile as profiled with Photogrammetry was very high and contained a high amount of detail, but remained time consuming and resource intensive. The Can-Can Machine produced profiles of the profiled terrains quickly and effectively. The Displacement Spectral Densities of the terrains profiled with the Can-Can Machine indicated that the resolution of the Can-Can Machine was high enough to obtain valuable information about the terrains. The conclusion is made that the Can-Can Machine is an accurate profilometer which profiles any terrain fast and cost effective.

The Displacement Spectral Densities of the profiled terrain are representative of the profiled terrain. The Displacement Spectral Density of each of the profiled terrains provided information about the terrains in the form of the Roughness Coefficient and the Road Index as well as the dominant frequencies generated when driving on the track. The Displacement Spectral Densities indicate that a straight line fit approximation on the Gerotek tracks does not include all of the track's characteristics.

The International Roughness Index was calculated for each of the profiled terrains and it indicated that the International Roughness Index was a valid method for characterizing smoother terrains.

6. 3-D road profiles in multi-body simulation models

The primary goal of this study was to obtain accurate 3-D profiles of actual test terrains used by the University of Pretoria. These profiles were required for the validation of mathematical models used in vehicle simulations. The MSC ADAMS simulation package is used by the University of Pretoria and thus the profiles were required to be described in terms of a MSC ADAMS Road Definition Files, also referred to as RDF files.

The ADAMS/3-D road models enable one to define an arbitrary three-dimensional smooth road surface, such as parking structures, racetracks and so forth. In addition, Adams/3-D Road lets you model three-dimensional road obstacles, which are placed on top of the underlying smooth road surface.

Road definition files can be created by defining the file type, file version and file format. Then the units of length, force, angle, mass and time are defined and the definition of the model method is set to 3-D after which the number of nodes is stated. The data points in the profile are known as nodes and presented by placing each node number followed by the x-value, y-value and z-value. Three nodes are used in defining each element in the road profile. The connectivity of the three nodes which define the element is defined in a clockwise direction. This is done to ensure that the orientation of each element is consistent. The definition of the road mesh is shown in Figure 102 and a blank example of the layout for a road definition file is supplied in Appendix C.

Road definition files were created with a program written in Matlab and were used for creating road definition files of the Belgian paving, fatigue track, parallel and angled corrugation tracks and the pothole track. All of these tracks were profiled with the use of the Can-Can Machine.

Road definition files were not created for the rough track and also not for the Ride and Handling track as these profiles were too large for the simulation programme to work with.

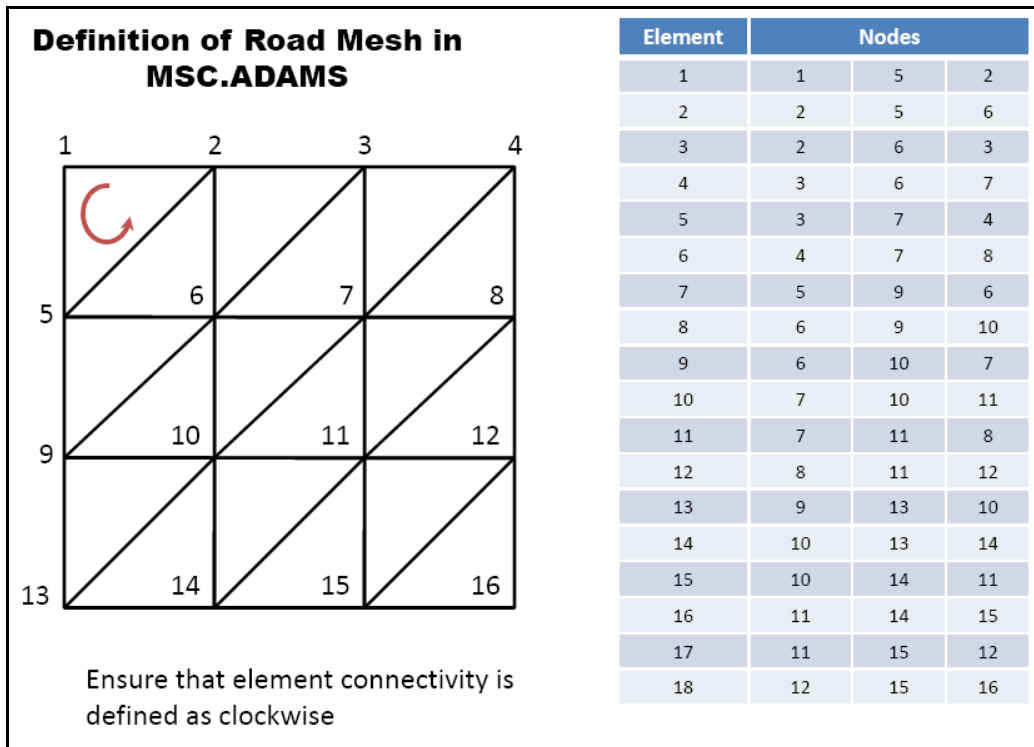


Figure 102: Definition of Road Mesh used in MSC ADAMS, (MSC Software, 2007).

6.1. Simulation and data verification

Proving ground test surfaces have been modelled as Finite Element models. The Finite Element models are modelled as shell elements with rigid material properties. The modelling of the road surface is important as the analysis duration depends on the contact simulation between the road surfaces and tyres. The road is often modelled as separate left and right surfaces to reduce the number of elements in contact with the tyre, as it reduces the solving time.

While generating a road surface for a simulation, sufficient length of smooth road surface needs to be provided at the start of the simulation. This enables the vehicle to stabilize before entering onto the proving ground, Edara (2005).

3-D contact analyses are useful for generating road load histories and stress and fatigue studies that require component force and acceleration calculation. These studies can help one calculate the effects of road profiles, such as potholes, curbs, or Belgian blocks.

Previous road surfaces used for vehicle simulations at the University of Pretoria was road surfaces modelled as separate left and right surfaces (Thoreson (2003), Els (2006) and Uys (2007)). With the availability of the ADAMS/3-D Road the requirement of full 3-D road surfaces increased. The accuracy of the Can-Can Machine has been established by the actual measurement and profiling of discrete obstacles. The following step was to

validate the road definition files created from the Can-Can profiled terrains. The validation of the simulation with the road definition file was done by comparing the measured response of the modelled Land Rover Defender 110 in the simulation, in the form of vertical accelerations, with the actual response of the Land Rover Defender 110 driving over the profiled terrain. The profiled terrain used in the validation was the Belgian paving.

The response of the actual Land Rover Defender 110 was measured with the use of accelerometers. An accelerometer was positioned inside on the body of the vehicle, below each of the rear passengers, as shown in Figure 103. Another accelerometer was located on the chassis, 300 mm in front of the front axle, as shown in Figure 104.



Figure 103: Placement of rear accelerometers in Land Rover Defender 110.

The response of the Land Rover was measured while driving over the Belgian paving at five different velocities namely, 15km/h, 26km/h, 40km/h, 57km/h and 73km/h. The velocity of the Land Rover was kept constant by driving against the governor in different gears.



Figure 104: Placement of front accelerometer on chassis of Land Rover Defender 110.

6.1.1. Simulations on the Belgian paving

Simulations were conducted at the required velocities in MSC.ADAMS/VIEW with the use of the previously validated model of the baseline Land Rover Defender 110. The validation of the model was conducted by Thoreson (2003).

Figure 105 indicates the layout of the front suspension system. The rigid axle is located longitudinally by leading arms connected to the vehicle body with rubber bushes. The stiffness of these bushes was measured and included in the ADAMS model. Lateral location of the axle is via a Panhard rod. The baseline vehicle is fitted with coil springs, translational dampers concentric with the coil springs and rubber bump stops. A steering angle driver is applied directly to the kingpin with a steering link connecting the left and right wheels. All other steering geometry is ignored in the model. The connections between the different components are indicated in Figure 106. To take the torsional stiffness of the ladder chassis into account, the vehicle body is modelled as two bodies connected to each other with a revolute joint along the roll axis and a torsional spring.

The rear suspension consists of a rigid axle with trailing arms, an A-arm, coil springs, translational dampers mounted at an angle outside coil springs and rubber bump stops. The basic layout is indicated in Figure 107. An anti-roll bar

is fitted to the rear suspension. The stiffness of the trailing arm rubber bushes is included in the ADAMS model. The schematic layout of the rear suspension is indicated in Figure 108.

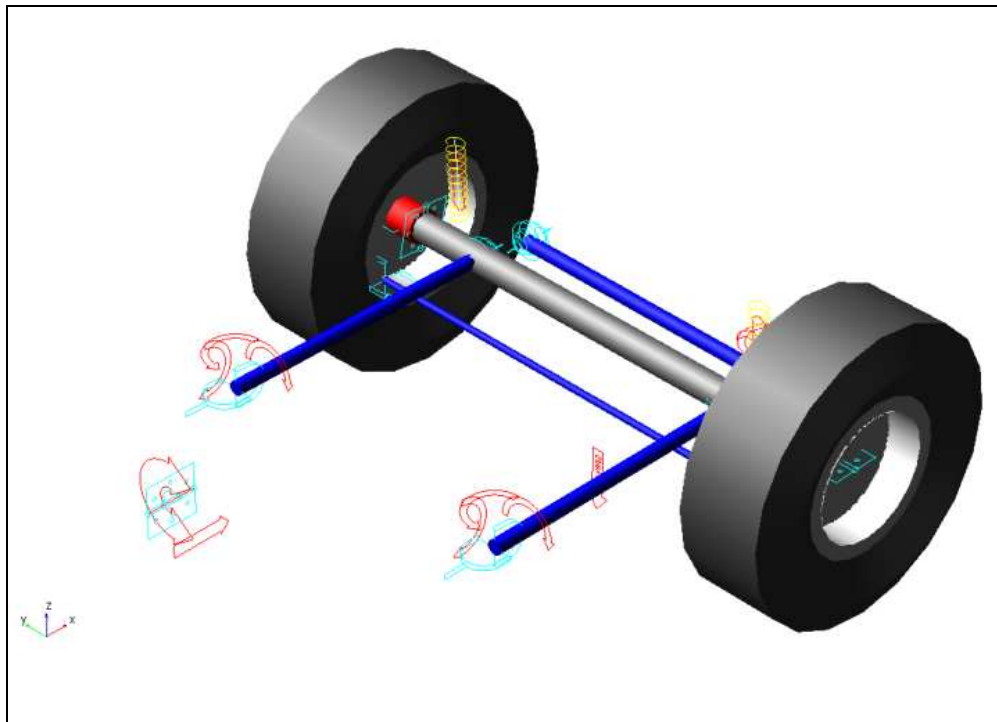


Figure 105: Front suspension layout.

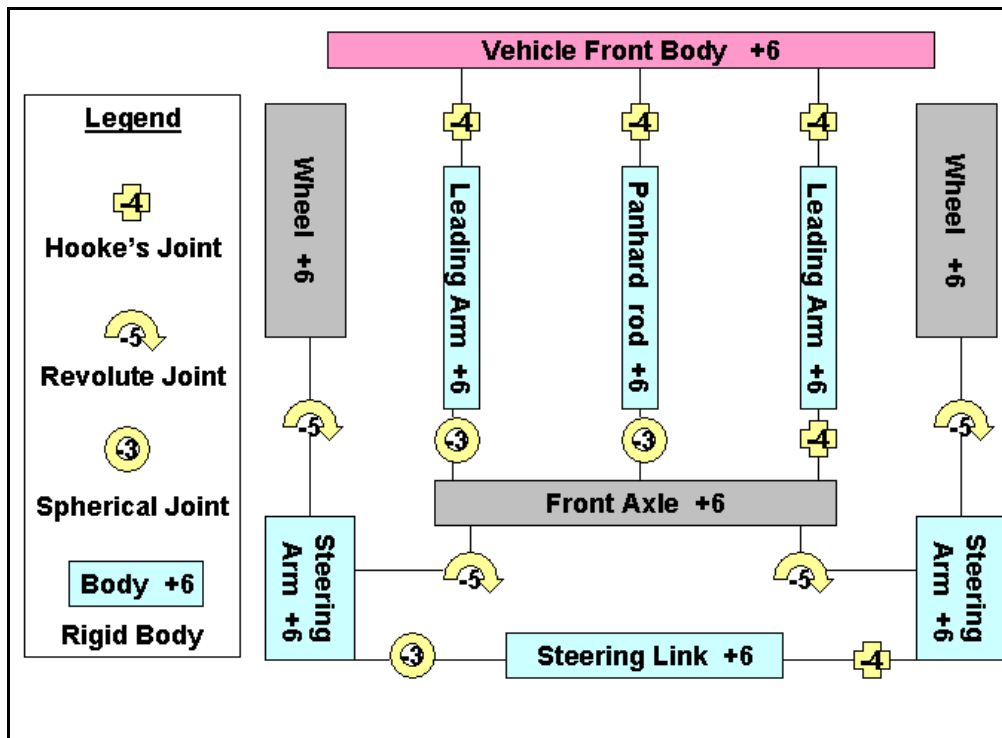


Figure 106: Front suspension schematic.

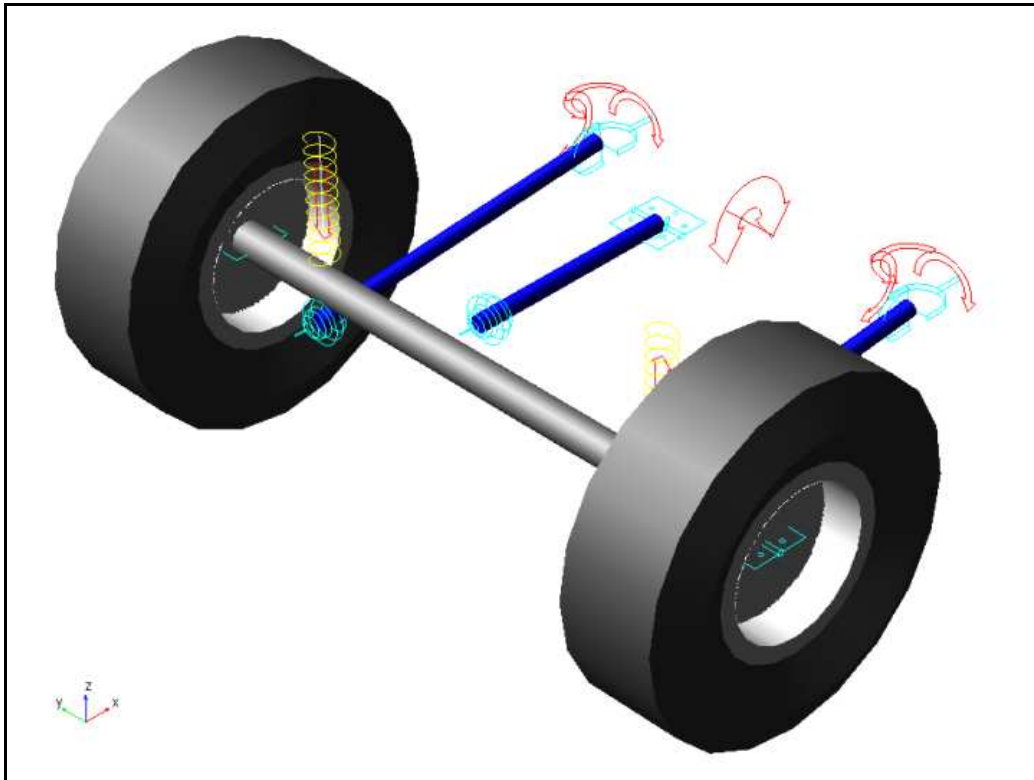


Figure 107: Rear suspension layout.

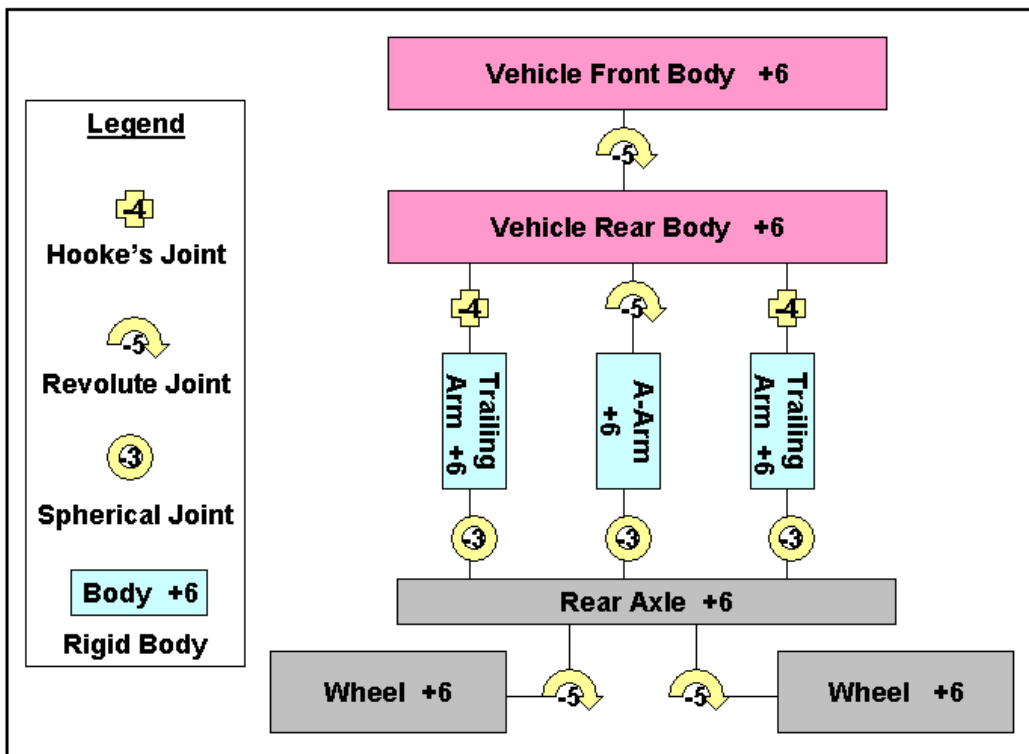


Figure 108: Rear suspension schematic.

Tyre side-force vs. slip angle characteristics were obtained from measurements using a two-wheeled tyre tester towed behind a vehicle. The measured data was converted to the coefficients required for the MSC ADAMS Pacjeka '89 tyre model. The tyre side-force vs. slip angle characteristics is indicated in Figure 109.

A Land Rover Defender 110 SUV was obtained locally for testing purposes. The aim of the baseline vehicle tests was to validate the ADAMS model of the vehicle and the tests were performed at the Gerotek Vehicle Test Facility.

The instrumentation used for the baseline tests, as well as measurement positions, is indicated in Table 3.

To validate the ADAMS model, simulation results were compared to measured results over a trapezoidal bump test. The vehicle driving over the trapezoidal bump is shown in Figure 110.

Test procedure and obstacle was chosen to ensure repeatability. Vehicle speed was kept constant by driving the diesel engine against its governor.

The vertical acceleration from the actual tests as well as the simulation results were weighted using the British Standard BS 6841, BS (1987), W_b weighting filter.

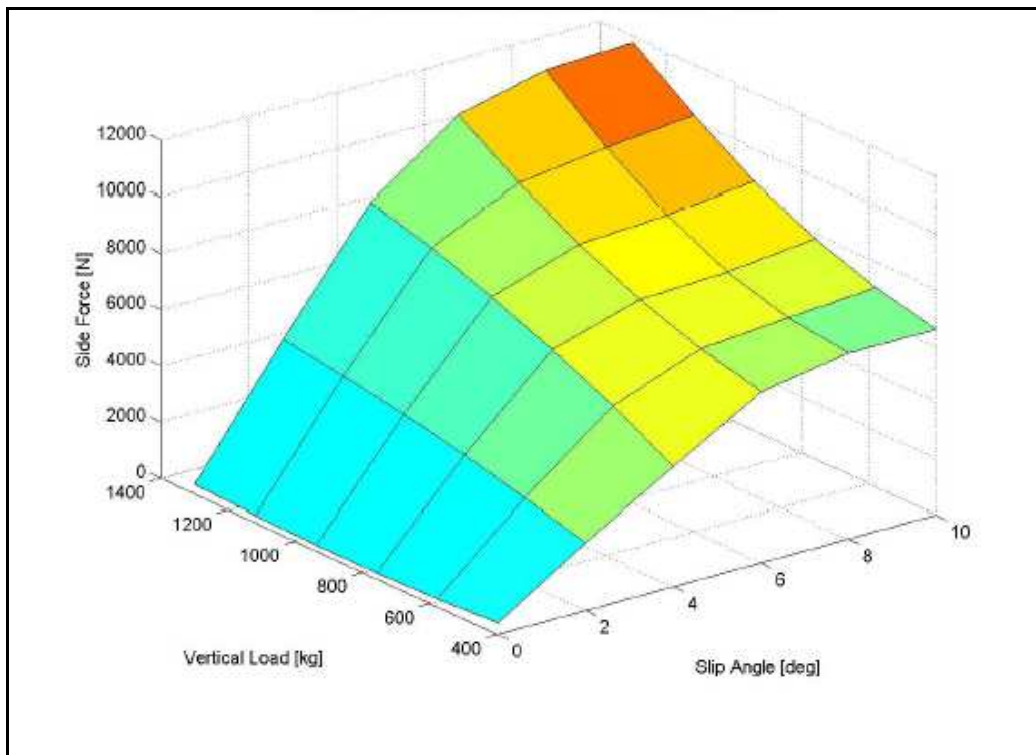


Figure 109: Tyre side-force vs. slip angle characteristic.

No	Parameter	Position	Equipment
1	Vehicle speed	Roof	VBOX GPS
2	Relative displacement	Left front suspension	Penny&Giles rope displacement transducer
3	Relative displacement	Right front suspension	Penny&Giles rope displacement transducer
4	Relative displacement	Left rear suspension	DWT rope displacement transducer
5	Relative displacement	Right rear suspension	DWT rope displacement transducer
6	Roll velocity	Vehicle body between front seats	Solid state gyro
7	Yaw velocity	Vehicle body between front seats (close to cg)	Solid state gyro
8	Relative displacement	Steering arm between axle and body	Penny&Giles rope displacement transducer
9	Acceleration	Left front lateral	Solid state accelerometer $\pm 4g$ range
10	Acceleration	Right rear vertical	Solid state accelerometer $\pm 4g$ range
11	Acceleration	Left rear lateral	Solid state accelerometer $\pm 4g$ range
12	Acceleration	Left rear vertical	Solid state accelerometer $\pm 4g$ range
13	Pitch velocity	Vehicle body between front seats	Solid state gyro
14	Kingpin steer angle	Kingpin	Potentiometer
15	Wheel speed	Left rear wheel	Turck Banner optical speed sensor
16	Driveshaft speed	Gearbox output rear	Turck Banner optical speed sensor

Table 3: Instrumentation used for baseline vehicle tests.



Figure 110: Trapezoidal Bump.

The trapezoidal bump was chosen to validate the vertical and pitch dynamics of the vehicle. The road input profile is easily measured and included in a

simulation model. Figure 111 indicates the correlation obtained between the measured and simulated results. Correlation is indicated for pitch velocity, spring displacement right front (rf), spring displacement rear left (rl), steering displacement as well as front and rear vertical accelerations. Correlation for vertical accelerations is especially good which is important because vertical acceleration is a direct measure of ride comfort. The model is thus considered validated for ride comfort simulation.

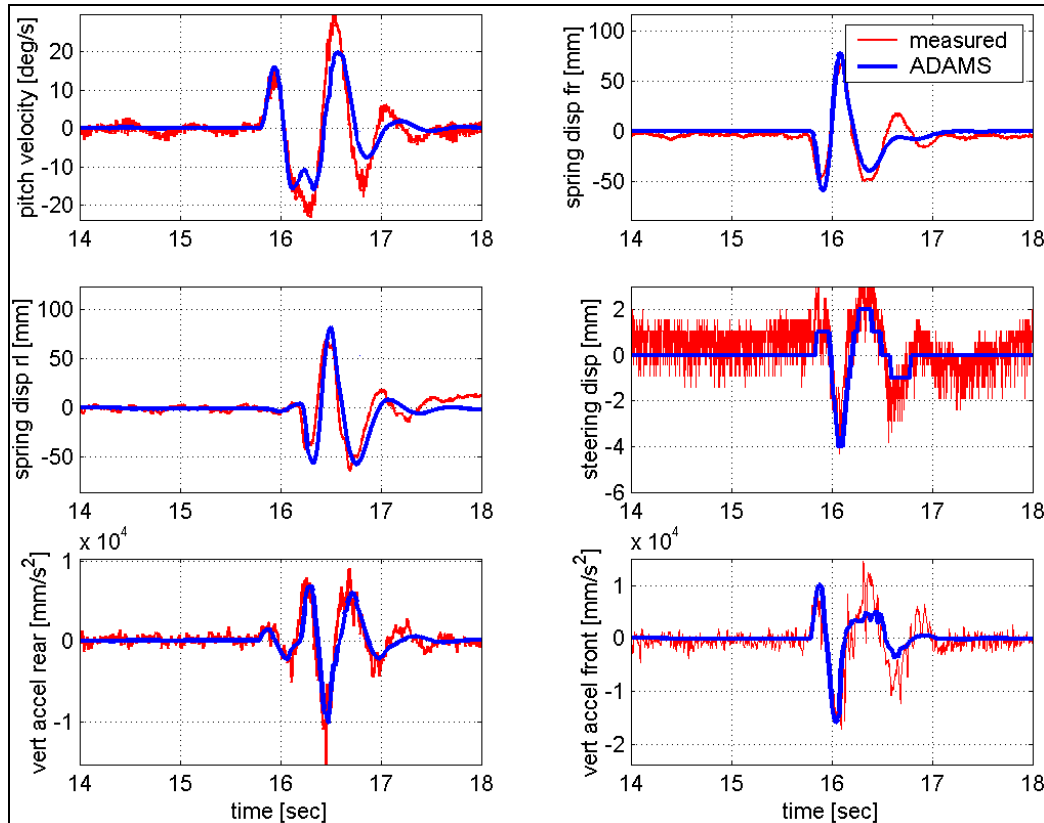


Figure 111: Model validation results for passing over 100 mm trapezoidal bump at 25 km/h.

The only adjustments made to the model, used for the simulations with the terrain profiles from the current study, were the addition of the 3-D Road Definition File and a steering driver was added which allowed the Land Rover to drive in a straight line over the terrain.

When simulating vehicle dynamics, the tyre model used is very important. ADAMS/Tire has a selection of tyre models which may be used of handling, ride, chassis control or durability simulations. Each tyre model is valid in a specific area and using a tyre model outside the specified area may result in non-realistic analysis. Table 4 indicates the preferred tyre model(s) to be used for a number of applications. In general the ADAMS/Tire Handling models are valid on rather smooth roads only. The wavelength of the road obstacles should not be smaller than the tyre circumference. If the wavelengths are shorter, the FTire model should be used which is able to cope with the non-linear tyre enveloping effects at high excitation frequencies.



Table 4: Typical applications for each tyre model (ADAMS/Tire, 2007).

MD	Event / Maneuver	ADAMS/ Handling Tire										Specific Models	
		PAC2002 ¹	PAC-TIME ¹	PAC89 ¹	PAC94 ¹	FIALA ¹	5.2.1.1 ¹	UA Tire ¹	PAC-MC ¹	FTire			
Adams	Stand still and start	+	o/+	o/+	o/+	o/+	o/+	o/+	o/+	o/+	o/+	o/+	+
	Parking (standing steering effort)	+	-	-	-	-	-	-	-	-	-	-	+
	Standing on tilt table	+	+	+	+	+	+	+	+	+	+	+	+
	Steady state cornering	+	+	o/+	+	0	0	o/+	+	+	+	+	o/+
	Lane change	+	+	o/+	+	0	0	o/+	+	+	+	+	o/+
	ABS braking distance	+	o/+	o/+	o/+	0	0	o/+	o/+	+	+	+	+
	Braking/power-off in a turn	+	+	0	0	0	0	0	+	+	+	+	o/+
	Vehicle Roll-over	+	0	0	0	0	0	0	0	0	0	0	+
	On-line scaling tire properties	+	-	-	-	-	-	-	-	-	-	-	0
	Cornering over uneven roads *	o/+	0	0	0	0	0	0	0	0	0	0	o/+
Ride	Braking on uneven road *	o/+	0	0	0	0	0	0	0	0	0	0	+
	Crossing cleats / obstacles	-	-	-	-	-	-	-	-	-	-	-	+
	Driving over uneven road	-	-	-	-	-	-	-	-	-	-	-	+
	4 post rig (A/Ride)	+	o/+	o/+	o/+	o/+	o/+	o/+	o/+	o/+	o/+	o/+	o/+
	ABS braking control	o/+	0	0	0	0	0	0	0	0	0	0	+
	Shimmy ²	o/+	0	0	0	0	0	0	0	0	0	0	+
	Steering system vibrations	o/+	0	0	0	0	0	0	0	0	0	0	+
	Real-time	+	-	-	-	-	-	-	-	-	-	-	-
	Chassis control systems > 8 Hz	o/+	-	-	-	-	-	-	-	-	-	-	+
	Chassis control with ride	-	-	-	-	-	-	-	-	-	-	-	+
Dura-bility	Driving over curb	-	-	-	-	-	-	-	-	-	-	-	o/+
	Driving over curb with rim impact	0	-	-	-	-	-	-	-	0	0	-	o/+
	Passing pothole	-	-	-	-	-	-	-	-	0	0	-	o/+
	Load cases	-	-	-	-	-	-	-	-	0	0	-	o/+
		-	-	-	-	-	-	-	-	0	0	-	o/+

* wavelength road obstacles > tire diameter
¹ use_mode on transient and combined slip
² wheel yawing vibration due to suspension flexibility and tire dynamic response

- Not possible/Not realistic
0 Possible
o/+ Better
+ Best to use

Some Handling Tyre models can describe the first order response of the tyre, but do not take the eigen frequencies of the tyre into account. This causes the Handling Tyre models to be valid up to approximately 8 Hz.

The Land Rover model used in ADAMS used the PAC89 ADAMS/Tire model which is a point follower together with the Pacejka '89 Magic Tyre Formula which calculates the forces in the tyre. The PAC89 tyre model was used for the validation of the Belgian paving Road Definition File since the model was previously validated with the Double Lane Change manoeuvre, (Thoresson, 2003), as well as for Vehicle Roll-over manoeuvres, (Uys, 2007). Table 4 indicates that with the use of the PAC89 tyre model, non-realistic analysis may be obtained. The Ftire model is the preferred tyre model to use for driving over uneven roads, however at the time an Ftire model and license was not available for the Land Rover Defender 110 model.

The model of the Land Rover driving over the Belgian paving is shown in Figure 112. In the figure the front wheels of the model are on the Belgian paving and the rear wheels are still on the smooth section of the terrain.

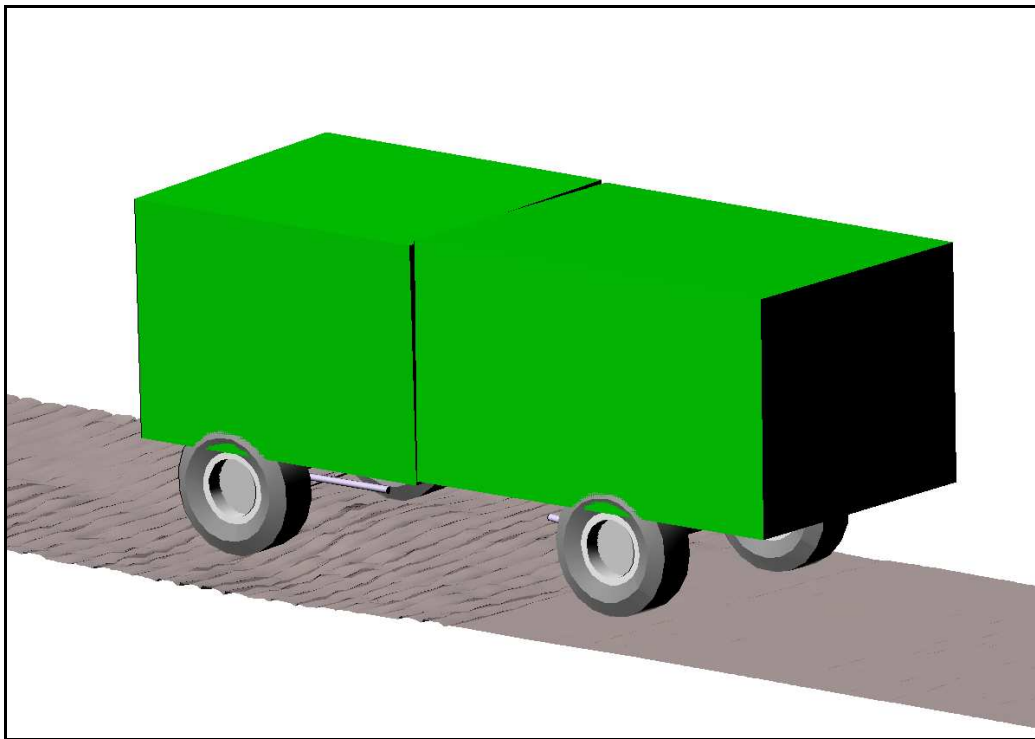


Figure 112: Model of Land Rover Defender 110 on the Belgian paving in ADAMS.

A close-up of the wire frame representing the wheel of the Land Rover and the mesh of the Belgian paving in ADAMS is shown in Figure 113. This figure illustrates the resolution of the terrain obtained with the use of the Can-Can Machine.

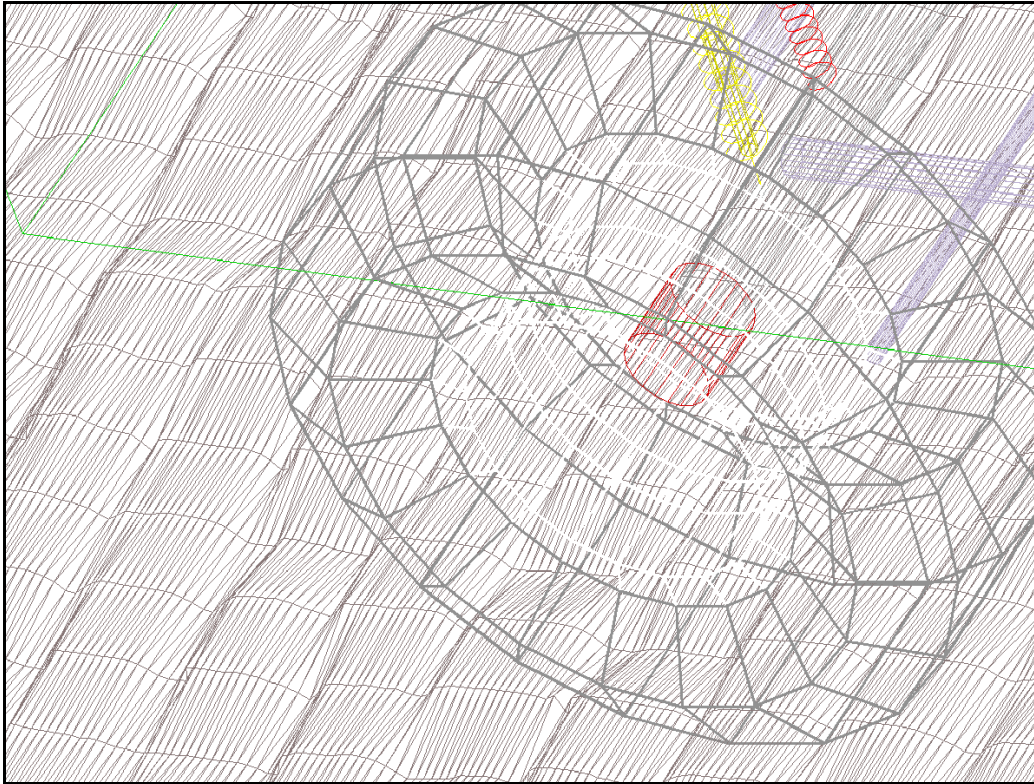


Figure 113: Close-up of the wire frame of the wheel on the Belgian paving mesh.

6.1.2. Simulation of Land Rover ride comfort

The ride comfort of the Land Rover was simulated over the Belgian paving road. Vertical accelerations at the three positions on the vehicle body were weighted using the BS 6841, BS, (1987) filter indicated in Figure 114. The BS 6841 standard is the British Standard Guide to measurement and evaluation of human exposure to whole-body mechanical vibration and repeated shock.

The Fast Fourier Transforms were calculated for the vertical accelerations of the three points of interest in the simulations as well as the vertical accelerations from the actual Land Rover measurements. The Fast Fourier Transforms were filtered with the weighting function prescribed by the BS 6841 standard (BS, 1987). An example of the weighted Fast Fourier Transform from the simulation and Land Rover data @ 40 km/h is shown in Figure 115. The weighted Fast Fourier Transform plots for all of the simulations and Land Rover data are available in Appendix E.

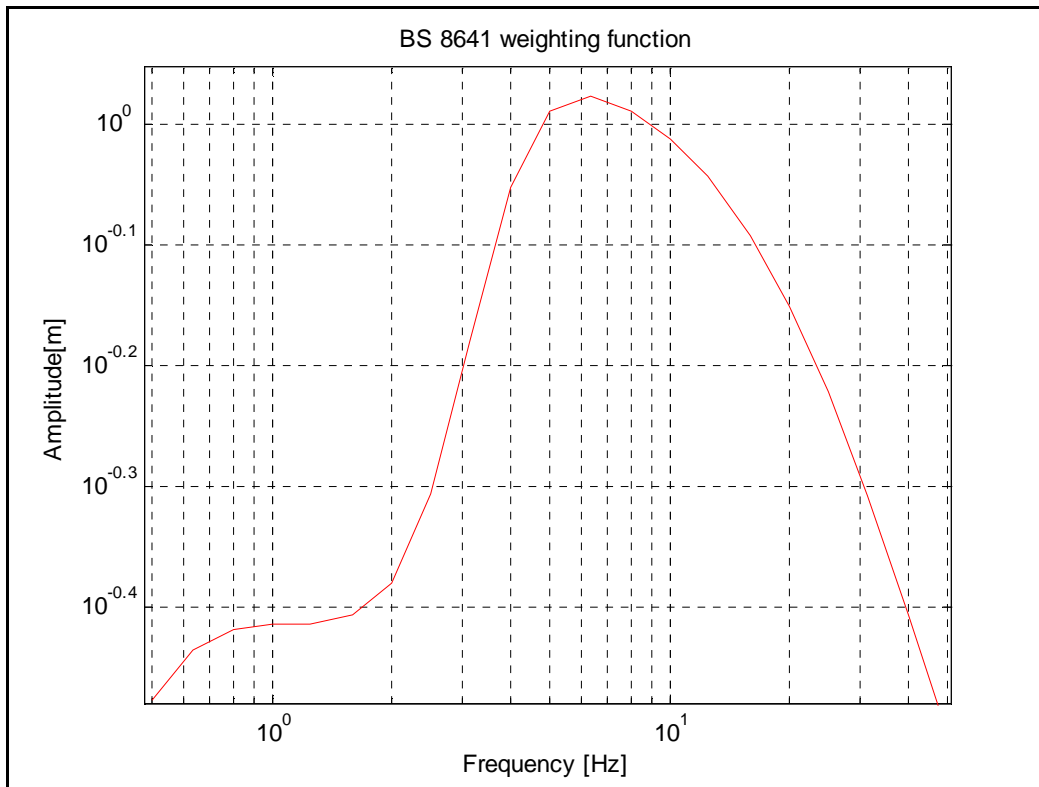


Figure 114: BS 6841 weighting function.

It can be seen in Figure 115 that there is good correlation between the simulation and Land Rover data up to approximately 8 Hz. This is expected due to the fact that the PAC89 Tyre model is valid up to approximately 8 Hz (see Table 4). Both measured and simulated data was subsequently filtered with an 8 Hz low pass filter and the resultant Fast Fourier Transform is shown in Figure 116. The 8Hz low pass filtered Fast Fourier Transform plots for all of the simulations and Land Rover data are available in Appendix E.

The Fast Fourier Transforms from the Simulations and the Actual Land Rover test data correlate very well. The trends and magnitudes of the Fast Fourier Transforms was the same and the peaks and valleys were found at the same frequencies.

The 8 Hz low pass filtered Fast Fourier Transforms were transformed back to the vertical accelerations in the time domain. The filtered vertical accelerations of the right rear body of the simulations and the actual Land Rover data @ 40 km/h is shown in Figure 117. The filtered vertical accelerations measured at the points of interest also correlate very well and it can be seen in Figure 117 that the trend of the accelerations were the same and the acceleration peaks were recorded at the same time. The filtered vertical accelerations of the three points of interest in the simulations and the Actual Land Rover data are presented in Appendix E. Direct comparison in the time domain is not possible because the chance that the vehicle followed exactly the same path (lateral position) during the simulation and actual tests are very slim.

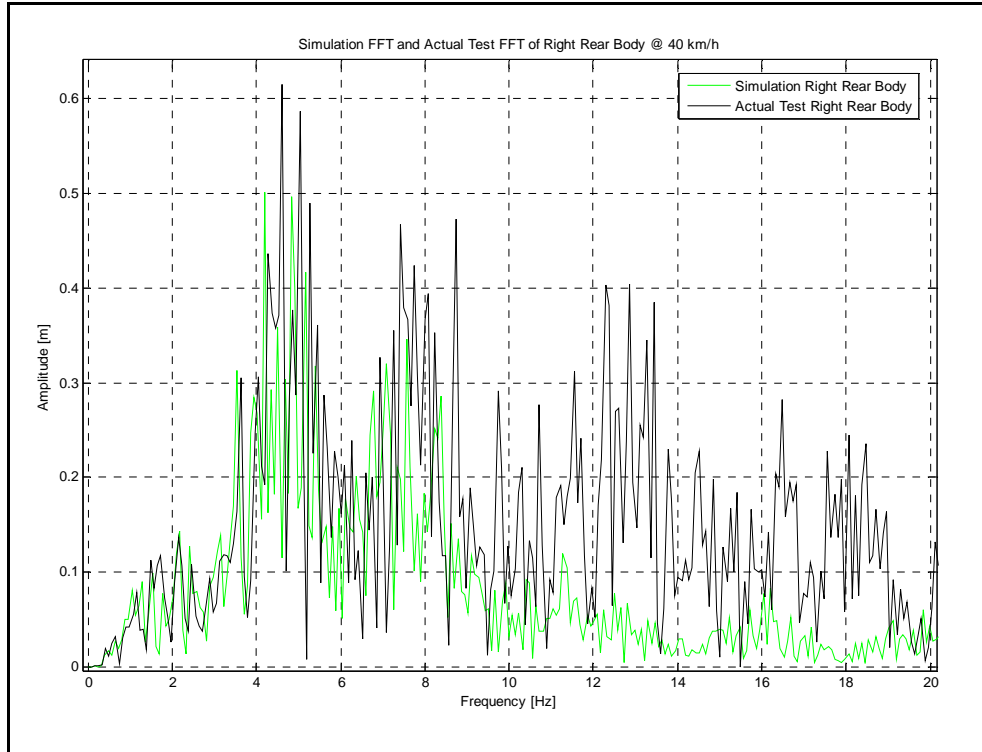


Figure 115: Weighted Fast Fourier Transforms of the Simulation and Land Rover data @ 40 km/h.

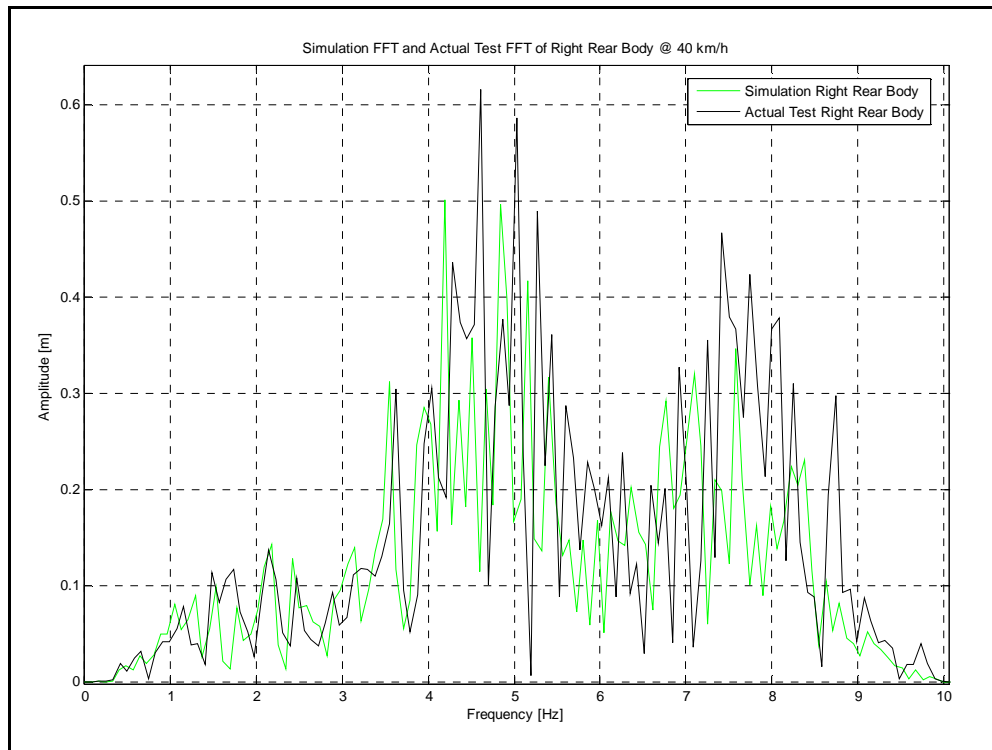


Figure 116: 8 Hz Low Pass Filtered FFT of the simulation and Land Rover data @ 40km/h.

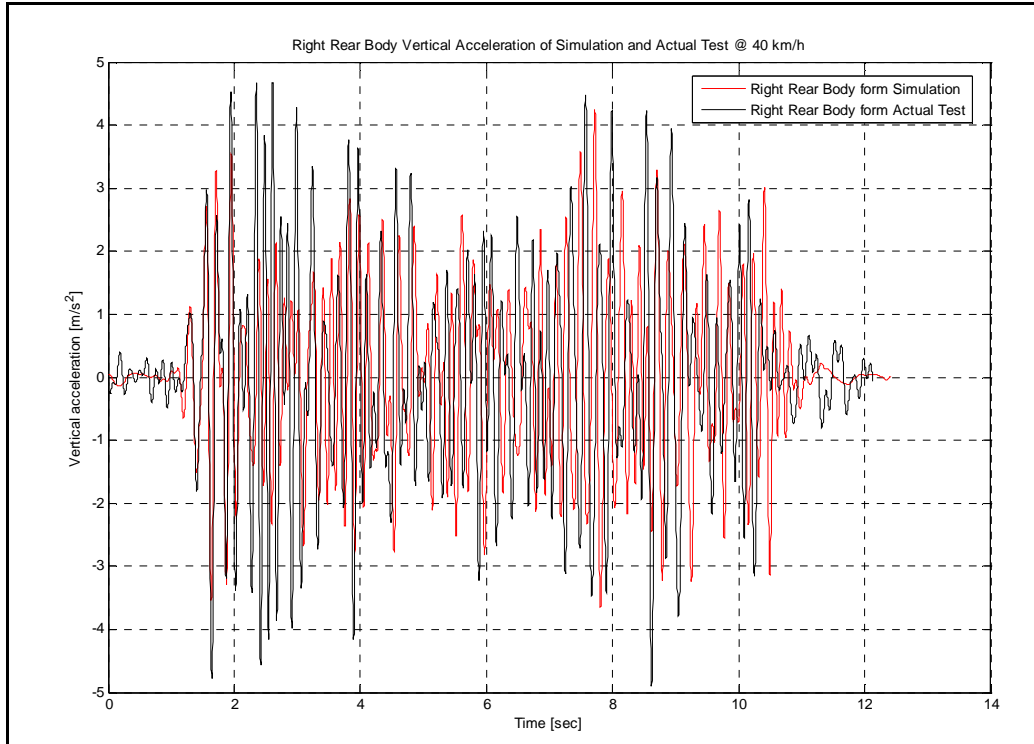


Figure 117: Filtered Right Rear Body vertical accelerations from simulation and Land Rover @ 40km/h.

The ride comfort of the occupants was therefore determined by calculating the Root Mean Square (RMS) value of the vertical acceleration. The Root Mean Square measures of acceleration may be used when the crest factor does not exceed 6. The crest factor of the motion is to be determined from the peak and RMS value of the acceleration after it has been frequency weighted.

$$\text{Crest factor} = \frac{\text{weighted peak acceleration}}{\text{weighted RMS acceleration}}$$

The peak and RMS values were determined over the full period of vibration exposure.

The RMS values of the three points of interest were calculated for the different speeds travelled in the simulations and the actual Land Rover. These values are graphically shown in Figure 118. It can be seen that the Left Front (LF) position in the simulation tends to measure higher accelerations than the same position on the actual Land Rover whereas the Right Rear and Left Rear (RR and LR) positions of the actual Land Rover tend to measure higher accelerations than the same positions in the simulations.

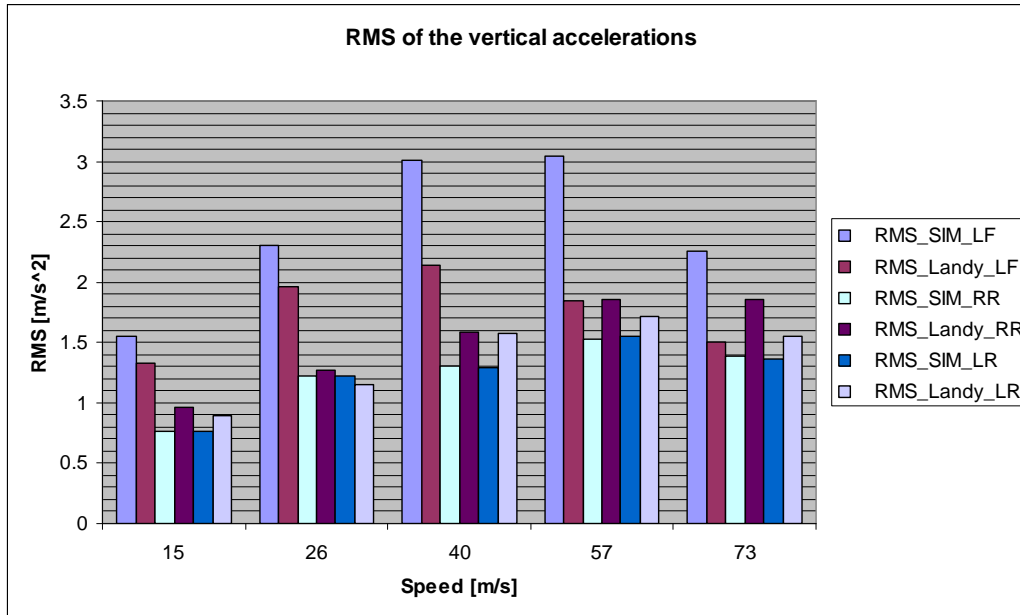


Figure 118: RMS values from Simulations and measured Land Rover data.

The higher accelerations and RMS values of the LF position in the actual Land Rover measurements was expected due to the fact that the accelerometer was placed on the chassis of the vehicle which in turn was exposed to additional accelerations caused by engine and driveline vibrations.

The higher accelerations and RMS values of the LF position in the simulations may have been due to the fact that the placement was 300 mm in front of the front axle which may be exposed to higher accelerations as the position was very close to the front of the vehicle.

The difference between the RMS values calculated from the vertical accelerations measured in the simulations and the vertical accelerations from the actual Land Rover is shown in Figure 119. It can be seen in Figure 119 that the best correlation between the simulations and the actual Land Rover is obtained at 26 km/h.

Simulated RMS values for LR and RR correlate well with the actual measurements and are generally within 20%. Correlation becomes worse as vehicle speed increases. This is attributed to the tyre model that only allows acceptable results up to 8 Hz, which excludes tyre hop. As vehicle speed increases, the terrain excitation moves to higher frequencies and the tyre model deficiencies become more pronounced.

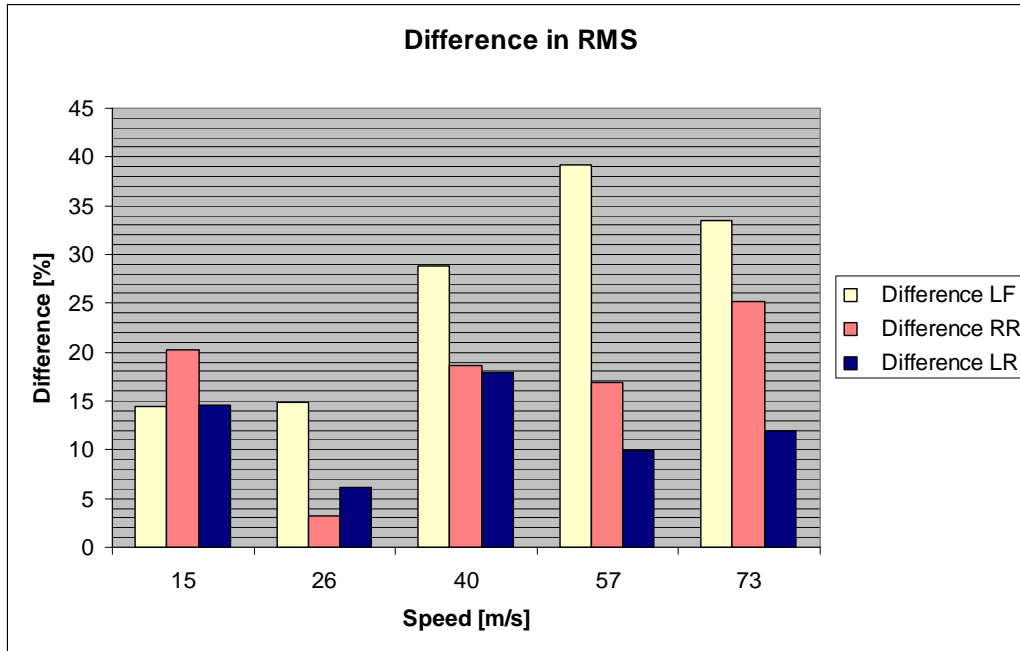


Figure 119: Difference in Simulations RMS values and Land Rover RMS values.

When compared to the RMS values in the BS code, the occupants' measured ride is very uncomfortable ($1.25 - 2.5 \text{ m/s}^2$) when driving over the Belgian paving, which is indeed the case.

6.2. Simulation and data verification

The conclusion is made that the 3-D profile of a terrain, profiled with the Can-Can Machine, was successfully implemented in a 3-D simulation of a Land Rover Defender 110 driving over the Belgian paving.

Good correlation between the response of the two rear points of interest in the simulation model and on the actual Land Rover indicates that the 3-D profile of the terrain is a valid and accurate profile of the actual terrain. The tyre model used in the simulations limited the results of the simulation. This limit was in the form of accurate and realistic analysis up to approximately 8 Hz. Improved analyses is possible with the use of an Ftire model. The Ftire model is fully nonlinear and provides accurate and realistic analysis in the frequency domain up to 120 Hz. The Ftire model was not used during this analysis due to the fact that an Ftire model for the Land Rover used in the simulations was not available.

The RMS values presented in Figure 118 and the difference in the RMS values from the simulations and the actual Land Rover shown in Figure 119 indicate that the correlation between the simulation and the actual Land Rover decreases as the speed of the vehicle increases. This is a direct result from

the PAC89 tyre model used in the simulations. This result is due to the fact that the PAC89 tyre model can only supply realistic analysis results up to approximately 8 Hz.

When the vehicle is travelling at 73 km/h and a realistic analysis can only be conducted at 8 Hz, very important data is lost between data points. This is the case because at 73 km/h the distance between data points is 2.5 m. It is also concluded that 73 km/h may also be too fast when calculating the RMS values for ride comfort on rough terrain. The calculation of the RMS value is very dependent on the correct travelling speed.

The best correlation between the simulation and the actual Land Rover was at 26 km/h where the difference in the RMS values at the three points of interest was 15% and lower.

Improved correlation may be obtained between the LF position in both the simulation model and the actual Land Rover if the LF position is moved to a position inside the vehicle and not directly on the chassis of the vehicle. This will reduce the effect of engine and drive train vibration on the measurement.

7. Conclusions and recommendations

7.1. Conclusions

To obtain an accurate profile of a terrain it is important to know the orientation of the profilometer when a terrain is profiled. Most of the terrains used for testing by the University of Pretoria have a known fixed reference around the terrain. The fixed reference is in the form of a flat surface around each terrain. Three profilometers were designed and built with the known flat reference in mind. The first profilometer was a mechanical profilometer (Can-Can Machine) on three wheels, each moving on the flat reference. The second profilometer profiled a terrain with the use of Photogrammetry. The third profilometer used a laser displacement sensor which was mounted in a gimball and positioned with stepper motors.

Photogrammetry and stereo techniques with aerial imagery is a possible option in profiling rough terrains. Although no literature was obtained where actual rough terrains were profiled with the use of Photogrammetry it remains a feasible option in the profiling rough terrains.

Laser scanning platforms are very accurate systems but the accuracy is compromised by the Global Positioning System when the 3-D model is placed in a global coordinate system. These systems have colossal raw data bundles and require state of the art computers for effective data processing. The laser scanning platforms are highly-priced and way beyond the resources for this study. The Laser scanning platforms are widely available however the vertical height required in order to profile a 100 m section of a terrain may compromise the obtainable resolution of the profile.

The proposed profilometers were reviewed and the operational functions of each were examined. Test sections were profiled with each of the proposed profilometers and the results were evaluated.

It was found that the Can-Can Machine is a simple and effective profilometer with the ability to profile rough terrain. The Can-Can Machine can profile a rough terrain with an accuracy of < 5 mm. The Photogrammetry profiling method is a valid and accurate profiling method with an accuracy of < 5 mm, however it remains time consuming and resource intensive. The Laser Scanner is a time consuming profilometer but remains a prospective profilometer still in the development phase. The Laser Distance Sensor has an accuracy of 5 mm but the accuracy of the total system is limited by the gimball.

The profiles obtained of the profiled terrains were accurate and visually very representative of the actual terrain. Although the resolution of the Laser Scanner was lower than the resolution of the Can-Can Machine a valid profile was still produced by the Laser Scanner. The resolution of the Belgian paving profile as profiled with Photogrammetry was very high and contained a high

amount of detail, but remained time consuming and resource intensive. The Can-Can Machine produced profiles of the terrains quickly and effectively. The Displacement Spectral Densities of the terrains profiled with the Can-Can Machine indicated that the resolution of the Can-Can Machine was high enough to obtain valuable information about the terrains.

The conclusion is made that the Displacement Spectral Densities of the profiled terrain were representative of the profiled terrain. The Displacement Spectral Density of each of the profiled terrains provided information about the terrains in the form of the Roughness Coefficient and the Road Index as well as the dominant frequencies generated when driving on the track. The values of the Roughness Coefficient and the Road Index were high as expected.

The International Roughness Index was calculated for each of the profiled terrains and it indicated that the International Roughness Index was a valid method for characterizing smoother terrains. The International Roughness Index of the rough terrains on which this present study were concentrating on indicated that the Displacement Spectral Density of the profiles were the superior method used in characterizing rough terrains.

When a 3-D tyre model is used in a simulation the mesh size of the road profile used for the simulation may not be larger than half the contact patch of the tyre. Thus one is able to use a road profile with a mesh size smaller or equal to 100 mm in the direction of travel.

Good correlation between the response of the two rear points of interest in the simulation model and on the actual Land Rover indicated that the 3-D profile of the terrain (as profiled with the Can-Can Machine) was a valid and accurate profile of the actual terrain. The tyre model used in the simulations limited the results of the simulation. This limit was in the form of accurate and realistic analysis up to approximately 8 Hz. Improved simulation analyses is possible with the use of an Ftire model. The Ftire model is fully nonlinear and provides accurate and realistic analysis in the frequency domain up to 120 Hz. The Ftire model was not used during this analysis due to the fact that an Ftire model for the Land Rover used in the simulations was not available.

The best correlation between the simulation and the actual Land Rover was at 26 km/h where the difference in the RMS values at the three points of interest was 15% and lower.

7.2. Recommendations for future work

It has been established that the Can-Can Machine is a fast, cost effective and accurate profilometer, however the following is suggested to improve the accuracy and operation of the Can-Can Machine:

- I. The use of multiple tilt sensors, one on the front and one on the rear of the Can-Can Machine, to determine the orientation of the structure of the profilometer. The multiple tilt sensors can be used to evaluate the front and rear movement of the structure.
- II. Stiffening the structure of the profilometer to enable the profilometer to move over rough terrain with ease.
- III. Increase the power delivered on the drive wheel to allow the profilometer to move over large obstacles without additional assistance.
- IV. A revision on the shape of the arms on the rear beam, which will allow the profilometer to profile large obstacles without the arms coming into contact with the obstacle.
- V. The accuracy of the Can-Can Machine in a global coordinate system can be increased with the addition of a RTK DGPS and an IMU to the Can-Can system.

Improved simulation analyses are possible with the use of an Ftire model. The Ftire model is fully nonlinear and provides accurate and realistic analysis in the frequency domain up to 120 Hz.

Improved correlation may be obtained between the LF position in both the simulation model and the actual Land Rover if the LF position is moved to a position inside the vehicle and not directly on the chassis of the vehicle. This will reduce the effect of engine and drivetrain vibration on the measurement.